ABSTRACT

Title of Thesis: INVESTIGATING CONTROLS ON NITROUS OXIDE DISTRIBUTIONS AND AIR-SEA FLUX IN SHALLOW TIDAL WATERS USING AN EFFICIENT, NON-TOXIC SAMPLING METHOD

Edward Andrew Hobbs, Jr. Master of Science Degree, 2019

Thesis Directed By: Dr. Jeremy M. Testa
Marine Estuarine Environmental Sciences

Nitrous oxide (N_2O) is a potent greenhouse gas that is naturally produced as a byproduct of nitrogen cycling. Eutrophication elevates nitrogen availability and enhances low-oxygen conditions, thus altering nitrogen cycling and associated N_2O availability, but a knowledge gap persists regarding controls on N_2O across estuarine environments. I studied three adjacent and nutrient-rich tidal tributaries of the Patapsco River (MD), one of which has engineered aeration (Rock Creek), to quantify how aeration and alterations to oxygen availability and nitrogen cycling will impact N_2O production. In all creeks, N_2O concentrations were above atmospheric levels and served as a source of N_2O to the atmosphere. Oxygen and nitrate availability were

most associated with variations in N_2O concentrations, and N_2O concentrations and air-water fluxes were highest in Rock Creek, especially during summer under non-aerated, but moderately oxygenated conditions. These new data help broaden our understanding of N_2O cycling, availability, and distribution within estuarine ecosystems.

INVESTIGATING CONTROLS ON NITROUS OXIDE DISTRIBUTIONS AND AIR-SEA FLUX IN SHALLOW TIDAL WATERS USING AN EFFICIENT, NON-TOXIC SAMPLING METHOD

by

Edward Andrew Hobbs, Jr.

Thesis submitted to the Faculty of the Graduate School of the
University of Maryland, College Park, in partial fulfillment
of the requirements for the degree of
Master of Science
2019

Advisory Committee:
Associate Professor Dr. Jeremy Testa, UMCES CBL, Chair
Associate Professor Dr. Laura Lapham, UMCES CBL
Associate Professor Dr. Lora Harris, UMCES CBL

Acknowledgements

I would like to first and foremost thank my primary advisor, Dr. Jeremy Testa for all of his support over the last two and a half years, as well as my committee member Dr. Laura Lapham, both of whom have taught me so much during over the two field seasons and hours spent in the laboratory. They have been instrumental in my development as a scientist and researcher, and have always had an open door when I needed guidance or direction. I would also like to thank my third committee member, Dr. Lora Harris, for her input and ideas throughout this project, and for her crucial involvement in planning and executing the field work that served as the basis for much of this project.

I would also like to thank the efforts of many faculty and staff from University of Maryland Center for Environmental Science Chesapeake Biological Laboratory for their efforts in sample collection and post processing, without which the information derived from this project would not have been possible. In particular, Casey Hodgkins, Melinda Forsyth, Erin Reilly, Amanda Moore, Nicole Basenback, Isabel Sanchez-Viruet, and Curtis Szewczyk were instrumental in helping with field work, maintaining laboratory equipment, running late night experiments, creating base maps and R code to help with data analysis, all the while making the process fun and enjoyable.

Additionally, I would like to thank Cedric Magen, Alyson Santoro (University of California, Santa Barbara), and Hugh Goldsmith (SRI Instruments) for their valuable contributions in troubleshooting the gas chromatograph used in this study as

well as the members of the Nutrient Analytical Services Laboratory for analyzing samples collected in this study. I would also like to thank the Restore Rock Creek community of Pasadena, MD for the continued support of ongoing research in the watershed as well as Anne Arundel County Department of Public Works for maintenance and control of the aeration system in Rock Creek that was a key aspect of this project.

I would also like to thank my parents and sister, who have fully loved and supported me over the last 26 years, and often acted as a sounding board. Their ongoing encouragement has been invaluable in my development as a person and scientist and I cannot thank them enough. I also thank all of my friends who have laughed with me and helped me in so many ways throughout this time. I would also like to thank my undergraduate mentors and advisors Dr. Karl Kehm, Dr. Christian Krahforst, Dr. Rebecca Fox, Dr. Leslie Sherman, and Martin Suydam who were, and continue to be, huge motivators in my work and decision to pursue a graduate degree.

Lastly, I would like to acknowledge the funding for this research provided by funds to PI Dr. Jeremy Testa from the Chesapeake Biological Laboratory, the Maryland Sea Grant Graduate Research Support Grant, the Explorer's Club Washington Group Exploration and Field Research Grant, and the National Science Foundation.

Table of Contents

List of Tables

Chapter 1

Chapter 2

List of Figures

Chapter 1

Chapter 2

correlations ($p<0.05$). Values within boxes represent correlation coefficients (Pearson method).

Figure 2.13 Relationship between N_2O concentration and DO concentration in surface and bottom waters in all creeks. Note significant correlation of N_2O and DO in bottom waters.

Chapter 1

Introduction

Nitrous oxide is a potent greenhouse gas that is naturally produced in marine and coastal environments as a byproduct of nitrogen cycling in the water-column and sediments (de Wilde et al., 2000; Ji et al, 2015). Atmospheric N_2O concentrations have increased significantly from ~270 ppb in preindustrial times to ~330 ppb in recent decades, and have been projected to rise with further human activity (Bange et al., 1996; Davidson, 2009; IPCC, 2013; Syakila & Kroeze, 2011, Thompson et al., 2019). The largest sources of N_2O emissions to the atmosphere are terrestrial and ocean ~11 TgN yr^{-1} and ~6 TgN yr^{-1}, respectively (IPCC, 2007; Thompson et al., 2019), but an increasing body of literature has documented elevated N_2O concentrations in upstream reaches of eutrophic estuaries (Barnes and Owens, 1999; Dong et al., 2004; Garnier et al., 2006; LaMontagne et al., 2003; Liu et al., 2015; Seitzinger et al., 1998), near oxygen minimum zones (Farías et al., 2009; Middelburg et al., 1995), and coastal waters (Bange et al., 1996; Barnes et al., 2011), relative to atmospheric equilibrium. Murray et al. (2015) estimates global estuarine ecosystems contribute 0.31 TgN yr^{-1} to the atmosphere via air-water N_2O flux. Although this contribution is an order of magnitude lower than terrestrial and oceanic N_2O fluxes, there is a growing interest in quantifying N_2O concentrations in the coastal zone, especially given the potential for increased nitrogen loading due to anthropogenic activities. Accurately quantifying nitrous oxide in estuarine waters is necessary to broaden our understanding of N_2O cycling, air-water flux, and distribution within

estuarine and coastal ecosystems, and can help constrain these terms for global climate models.

A common technique to measure nitrous oxide in estuarine waters involves equilibrating sample water with a nitrogen gas (N_2) headspace following the addition of mercuric chloride ($HgCl_2$), which preserves the sample until the headspace gas can be injected into a gas analyzer (Bange et al., 2001; Brezonik & Lee, 1966; Cooper, 1933; Elkins, 1980; Ji et al., 2018; Wilson et al., 2018). The addition of $HgCl_2$ to water samples is a generally accepted preservation method, as it sufficiently arrests biological activity in samples until they can later be analyzed in a laboratory (e.g. Wilson et al., 2018). For this reason, $HgCl_2$ is used in the analysis of various chemical measurements such as alkalinity, dissolved organic carbon (DOC), and dissolved gases such as nitrogen, oxygen and argon. The use of $HgCl_2$ for sample preservation has several environmental and safety disadvantages, however, in that it can be dangerous to the individuals collecting the samples to handle $HgCl_2$ and storage and disposal of $HgCl_2$ creates the potential for environmental contamination and/or costly disposal. In addition, water samples collected for trace metal analyses (especially Hg) may also be contaminated if $HgCl_2$ is not properly contained and is used in close proximity to the sampling activity.

Despite the widespread application of $HgCl_2$ as a preservative for various analyses and the associated drawbacks of using the toxic chemical, there is a sparsity of literature that details the analytical testing, precision, and necessity of using $HgCl_2$ for collecting water samples to be analyzed for N_2O concentrations. In a study by Yoshinari (1976), water samples were collected both with and without $HgCl_2$ addition

from numerous depths in the Gulf Stream water column between Halifax and Bermuda, and the resulting N_2O concentrations from preserved and unpreserved samples were compared. In general, the N_2O concentrations yielded ~3% variability between duplicate samples and there did not appear to be a consistent difference in N_2O concentrations between the $HgCl_2$ preserved and unpreserved samples. There were large discrepancies between the preserved and unpreserved samples within samples from the Oxygen Minimum Zone (OMZ), however, where N_2O concentrations in the unpreserved samples collected at this depth were over twice as high as those fixed with $HgCl_2$. While this difference could result from biological N_2O production in the unpreserved samples, these samples were not analyzed until one month after collection. This delay to analysis may have allowed for biological activity within the water sample to alter the N_2O concentrations. Given the numerous disadvantages of using $HgCl_2$ as a preservative and the lack of literature justifying the method as the benchmark for N_2O concentration analysis, alternative sampling and measurement methods that minimize analytical and sample error, but avoid the use of $HgCl_2$ and its associated handling and disposal protocols would benefit the community interested in N_2O measurements.

In the chapter that follows, we present an alternative method for collecting samples for nitrous oxide concentration analysis via an *in situ* headspace extraction (ISHE) that does not require the addition of a toxic or caustic preservative, and eliminates the need to store sample water until laboratory analysis. Eliminating the necessity for a hazardous preservative and increasing the convenience and efficiency of sample collection may facilitate more frequent N_2O measurements to further our

understanding of N_2O generation in estuarine and coastal systems. We compared the accuracy and precision of the ISHE technique to the $HgCl_2$ preservation method and demonstrate that it serves as a robust alternative at N_2O concentrations higher than atmospheric levels in waters with estuarine salinity (0-25). We then apply the method across a diverse range of environmental conditions in Chesapeake Bay, where N_2O measurements have previously been scarce.

Sampling Locations and Environments

All sampling and method comparisons were performed in the Patuxent River estuary in Maryland, USA, which is a tidally influenced tributary of Chesapeake Bay that experiences nutrient loading from point and non-point sources and has been a site of intense long-term monitoring and measurement programs (e.g. Testa et al. 2008, Boynton et al. 2008). Salinity ranges from zero in tidal freshwater in the upper regions to mesohaline (10-18) near the mouth of the river (Boyton et al., 2008; Breitburg et al., 2003; Testa and Kemp, 2008). The watershed is primarily forested, with forested and agricultural components (Boynton et al. 2008, Fisher et al., 2006, Homer et al., 2007). Tidal freshwater marshes are present in the upper section of the river, which is vertically well-mixed, has a mean depth of 1.1 m, and experiences high turbidity (Boynton et al., 2008; Williams et al., 2006). The lower portion of the estuary undergoes seasonal stratification where depths average 5.4 m (Boynton et al, 2008) and a deep channel reaches anoxic levels in the summer (Breitburg et al., 2003; Testa and Kemp, 2008). A long term Patuxent River monitoring program has been in place at the CBL Research Pier since the 1930s measuring salinity and water temperature and since 2003, temperature, salinity, and dissolved oxygen have been

measured continuously (every 15 minutes). Recently, the historical Pier Monitoring program has been supplemented by measurements of dissolved and particulate nutrients (N, P, Si), chlorophyll-a, total suspended solids, and community respiration rates on a bi-weekly basis. This long term monitoring was recently extended to include four additional stations that span the tidal axis of the river from freshwater (upriver) to mesohaline (downriver) conditions that were visited three times a year during May-September in 2018 and 2019. These different platforms were utilized to capture a diversity of physical and chemical conditions during the comparison of ISHE and $HgCl_2$ preservation techniques described in this chapter.

Samples for N_2O analyses and methods comparison were collected from five locations on the Patuxent River (PAX) estuary and analyzed at Chesapeake Biological Laboratory (CBL) (Figure 1.1). Surface and bottom water samples were collected in triplicate from the CBL research pier once in March and twice in July 2019 using both the ISHE and $HgCl_2$ methods. Additional samples were collected from Patuxent River Stations 1, 2, 3, and 4 in late July when anoxic conditions were present in bottom waters of downriver stations. Samples were collected from two depths (surface and bottom) at upriver stations 1 and 2, and at five depths in downriver stations 3 and 4. ISHE samples were collected in triplicate and $HgCl_2$ samples in duplicate during this Patuxent River cruise.

Materials and procedures

Materials

A 1ppm N_2O in N_2 certified calibration standard was purchased from Roberts Oxygen and diluted with appropriate volumes of ultra high pure (UHP) N_2 gas to create standards of 0 ppm, 0.3 ppm ± 3%, 0.5 ppm ± 3%, 0.7 ppm ± 3%, and 1 ppm ± 3%. The 140mL non-sterile monoject piston syringes with luer lock tip (#8881114030) used for ISHE sample collection were purchased from Mountainside Medical Equipment. The 1 cm thick black butyl rubber stoppers were purchased from Geo-Microbial Technologies (#1313) and the 20 mm aluminum seals used to cap the 10mL glass serum vials from Wheaton (#224183-01). The 10mL glass serum vials for the ISHE method (#223686IP) and 125mL glass serum bottles (#223748) for $HgCl_2$ method were also purchased from Wheaton. BD provided the 10mL non-sterile luer lock tip syringes for the $HgCl_2$ technique (#301029) as well as 22G PrecisionGlide hypodermic needles. The 3-way male luer lock stopcocks utilized in both methods were purchased from Cole-Parmer (EW-30600-25). The 1 mL Norm-Ject syringes with luer lock tip were purchased from Henke Sass Wolf (#4010-200V0). The 30 gL^{-1} saturated $HgCl_2$ solution was created with 99.5% $HgCl_2$ pellets from Acros Organics (#201430250) and ultrapure water from a Barnstead Pacific RO (reverse osmosis) coupled to a Barnstead Nanopure water system.

Procedures

Water sampling procedure – $HgCl_2$ preservation

Surface and bottom water samples from the CBL Pier were collected using a Rule Industries 1500 GPH electric bilge pump fitted with a garden hose and Nalgene PVC tubing. Samples taken during the Patuxent River cruise were collected from Niskin bottles mounted on a SeaBird SBE 55 Eco rosette array with six 4-liter Niskin bottles. Nalgene PVC tubing was attached to the spigot on the Niskin bottles and water was flushed through the tubing to ensure there were no bubbles in the sample water. The tubing was placed in the bottom of the 125 mL glass serum bottles, which are flushed with three volumes of water to ensure no bubbles are introduced to the sample. As the bottles are filling, the plunger from a 10mL plastic syringe was removed and the empty syringe was fitted with a 3-way stopcock and needle, which was then used to puncture a butyl rubber stopper. The tubing was slowly removed from the 125 mL glass bottle to prevent bubble formation. The punctured stopper was then inserted into the top of the 125 mL bottle and capped. Water displaced by the insertion of the stopper escapes through the needle and into the empty syringe to maintain a sample pressure of 1 atm. The excess water in the open syringe provides a water seal to prevent atmospheric contamination during sample preservation. A plunger was inserted into the syringe and the stopcock was opened so that the excess water displaced during the capping of the 125 mL bottle was expelled without being injected into the sample.

Next, a syringe preloaded with greater than 10 mL UHP N_2 is fitted with a 3-way stopcock and needle and excess N_2 is expelled until 10 mL remains in the

syringe. This syringe is then used to puncture the rubber stopper of the 125 mL bottle. A headspace is added to the 125 mL bottle 10 by inverting the bottle and injecting the UHP N_2. This 10 mL N_2 addition displaces 10 mL sample water into the secondary empty syringe and prevents overpressurization of the sample bottle. Both syringes are then slowly removed from the septa and the aluminum cap is crimped to prevent the septa from dislodging as a result of sample transport and/or thermal expansion of water. A 1 mL syringe was then fitted with a needle and filled with 300μL of 30 g L^{-1} $HgCl_2$ which was then injected into the bottle to preserve the sample until analysis. Samples are then double bagged and placed upside down in a cooler to create a water seal and prevent possible contamination from atmospheric air. $HgCl_2$ preserved samples do not require temperature-controlled environments as the biological activity that may affect N_2O concentrations within the sample water is arrested after the addition of $HgCl_2$. The $HgCl_2$ preserved samples are also equilibrated to the temperature of the laboratory prior, which is used when calculating the solubility and concentrations of N_2O, and shaken for two minutes to equilibrate the headspace with sample water prior to analysis. A sequence of sampling steps is shows in Figure 1.2.

Water sampling procedure – ISHE technique

CBL Pier water was collected with the bilge pump and Patuxent River cruise water was collected with the Niskin bottles using tubing flushing methods as described in the previous section. For collection of samples involving the bilge pump, water is collected from a two-gallon bucket that is filled from the bottom and flushed with three volumes of water and water temperature is recorded. In both water collection scenarios, a 140 mL syringe equipped with a 3-way stopcock is preloaded

with greater than 20 mL of UHP N_2. The expulsion of the excess N_2 serves to flush the 3-way stopcock prior to sample collection. The 140 mL syringe is then filled with 120 mL sample water and shaken for two minutes to equilibrate the 20 mL N_2 headspace with the sample water. After the two-minute equilibration period, 50 mL of sample water is expelled from the 140 mL syringe into a small plastic cup and the temperature of the water in the cup is recorded. This temperature is necessary to record as it is a key component in accurately quantifying N_2O solubility and concentration during laboratory analysis. A five-gallon bucket is filled with water typically collected from the sample station during this period. A 10 mL glass serum vial is then submerged in the five-gallon bucket and allowed to fill with water. The 140 mL syringe is inverted so that the stopcock is facing upwards and submerged in the five-gallon bucket. The 10 mL vial is then positioned such that the open end is located directly above the stopcock of the 140 mL syringe. The plunger of the 140 mL syringe is slowly pushed inwards to expel the equilibrated headspace, which displaces the water in the 10 mL vial, leaving only the headspace in the vial. The 140 mL syringe is removed from the bucket and a black butyl rubber stopper is submerged. Keeping the 10 mL vial upside down so that the headspace does not escape, the rubber stopper is inserted and the vial is sealed. The 10 mL vial with equilibrated headspace is then removed from the five-gallon bucket and an aluminum cap is crimped to prevent unintentional removal of the septa during sample transport. ISHE sample vials are then bagged and placed in a storage container. Each bag is filled with water to isolate the extracted headspace and glass serum vial from ambient air, eliminating the potential for atmospheric contamination. ISHE samples do not

need to be stored in a temperature-controlled environment. A sequence of sampling steps and images of the process are shown in Figure 1.3 and 1.4, respectively.

Calibration standards and standard curve

All samples and standards were analyzed for nitrous oxide using an SRI Instruments Gas Chromatograph (GC) with Electron Capture Detector (ECD) 8610C with UHP N_2 carrier gas (GC settings can be found in Table 1.1). Calibration standards were created each day and a five-point linear standard curve was generated using the Roberts Oxygen 1 ppm N_2O in N_2 certified standard and UHP N_2. Analytical precision of the instrument at 1 ppm N_2O is ± 3%, determined by repeated analysis of a certified standard from Roberts Oxygen. The standard curve was generated on a daily basis to establish a linear response of the GC to the calibration standards. Standards of 0 ppm, 0.3 ppm, 0.5 ppm, 0.7 ppm, and 1 ppm were run as part of the five-point standard curve at the beginning and end of each day. Standards were run in triplicate or until the coefficient of variance (CV) was ≤ 3% for each standard. Correlation thresholds (R^2) ≥ 0.99 are considered acceptable for calibration curves in this study.

Brine solution

A brine solution is injected into both ISHE and $HgCl_2$ preserved samples vials in order to displace the equilibrated headspace needed for GC analysis. To do so, 5 mL of the NaCl saturated brine solution previously degassed with UHP N_2 is injected into the vials to displace 5 mL of the equilibrated sample headspace into a syringe. It is necessary for the brine solution to be NaCl saturated to ensure no background N_2O

is present in the solution that could contaminate the sample headspace during displacement. The 5 mL brine addition and simultaneous 5 mL headspace displacement also prevents overpressurization of the sample that could alter N_2O solubility. In order to confirm whether or not the brine solution was not contaminated with N_2O, the solution was tested each day that samples were analyzed. An average brine partial pressure of 0.033 ppm N_2O was established (n=33), demonstrating that the brine solution was not completely devoid of N_2O, but was ~9 times lower in partial pressure than the lowest standard run for the daily calibration N_2O curve (0.3 ppm). These brine blanks were extracted in the same manner utilized for ISHE sample analysis.

Chemical analyses – $HgCl_2$ preserved samples

All samples collected for N_2O measurement were analyzed at Chesapeake Biological Laboratory using the SRI GC-ECD. Samples preserved with the $HgCl_2$ spike method were stored at room temperature (21^{o}C) after collection and transport. Prior to headspace extraction, 5 mL of saturated NaCl brine solution was extracted from the Büchner flask via a 10 mL plastic syringe fitted with a 3-way stopcock and 22G needle. A secondary 10 mL syringe fitted with a 3-way stopcock and needle was flushed with UHP N_2 gas. The 5 mL brine solution was then injected into the 125 mL sample bottle preserved with $HgCl_2$ and 5 mL of equilibrated headspace was displaced into the secondary N_2 flushed syringe to maintain equilibrium pressure of 1 atm. The syringe filled with 5 mL of the equilibrated headspace was then removed from the septa of the glass bottle, the needle was detached, and the headspace was injected into a 1 mL sample loop on the SRI GC-ECD for analysis.

Chemical analyses – ISHE preserved samples

The headspace extraction method for ISHE preserved samples follows the same process as the $HgCl_2$ preserved extraction method with the 5 mL volume of brine solution injected into the 10 mL ISHE vial while a secondary N_2 flushed syringe is attached and filled with displaced headspace prior to GC analysis.

Calculations

N_2O concentrations were calculated from the GC measurements, the ideal-gas law, and gas-specific coefficients via the following equation (Walter et al. 2006):

$$C_{N_2O} = \frac{F\ x\ P\ V_W + \frac{x\ P}{R\ T} V_h}{V_W} \quad (1)$$

where C_{N_2O} is the concentration of N_2O in nmol L^{-1}, F is the solubility function coefficient for nitrous oxide that accounts for non-ideal conditions in nmol L^{-1} atm^{-1} (Weiss and Prince, 1980), V_w and V_h are the respective volumes of the sample water and headspace in L, x is the dry gas mole fraction of N_2O in the headspace in ppb, P is the atmospheric pressure in atm, R is the gas constant of 0.08206 in L atm mol^{-1} K^{-1}, and T is the equilibration temperature in K. The solubility coefficient F is calculated as a function of *in situ* salinity and temperature, and solubility coefficients of N_2O in mol L^{-1} atm^{-1} (Weiss and Price 1980).

Assessment

Internal standard accuracy

An intercalibration standard (326.5 ppb reported partial pressure) utilized in Wilson et al. (2018) was analyzed on the GC on three separate days to validate the accuracy and precision of the linearity of the GC response (Figure 1.5). The standard was run in triplicate and yielded CVs of 0.9, 2.5, and 2.6 for the three days in which it was analyzed. The N_2O concentration of the intercalibration standard was calculated using the integrated peak value and the linear equation generated by the daily standard curve. Calculated partial pressure was within 3.4% of the reported value based on the average calculated partial pressure from three separate standard curves (Table 1.2). These results indicate our instrument meets the intercalibration standards of Wilson et al., (2018), which reported up to 27% variability in trace N_2O measurements between laboratories involved in the study.

Analytical considerations and limit of detection

Analytical precision (± 3%) and accuracy capabilities of the GC response are robust but there are considerations to be addressed for understanding how to quantify and establish analytical limits. Limit of quantitation (LOQ), defined as the lowest concentration that an analyte can be confidently measured (Armbruster & Pry, 2008), is a conservative analytical limitation metric and is set to 0.3 ppm (partial pressure of the lowest standard run for a daily calibration curve) for this study. Limit of blank (LOB) and limit of detection (LOD) were calculated for a singular day of analyses to provide an estimate of these less conservative limitations using the following

equations (Arumbruster & Pry, 2008):

$$LOB = \text{mean}_{blank} + 1.645(SD_{blank}) \quad (2)$$

$$LOD = LOB + 1.645(SD_{concentration\ sample}) \quad (3)$$

The limit of blank was calculated using the brine blank mean and standard deviation (see *Brine solution*) and was 0.054 ppm and limit of detection was 0.067 ppm. Average LOB and LOD may be calculated for numerous days of analysis, but is not required as the more conservative LOQ is utilized for the purpose of this study. Thus, samples yielding N_2O partial pressures under 0.3 ppm are currently considered below the limit of quantitation of the GC for this study and cannot be confidently reported, but the < 0.1 ppm LOB and LOD indicate that the instrument is capable of measuring much smaller concentrations.

Testing equilibration time

A necessary component of dissolved gas sampling is to fully equilibrate headspace with sample water prior to GC analysis. Various equilibration periods were tested to determine the minimum time required for full headspace equilibration for the ISHE technique. Studies analyzing dissolved gasses typically equilibrate a headspace with sample water via a period of physical agitation, but these times vary. Wilson et al. (2018) reports equilibration times between laboratories involved in the intercomparison study ranging from 20 minutes to 24 hours for samples that are not agitated. Some studies report physical agitation periods as little as 2 and 5 minutes

(Elkins, 1980; Magen et al., 2014), while others shake for 2 hours to equilibrate the sample (Laperriere et al., 2018). Shorter equilibration periods for the ISHE method are desirable because sample collection time in the field is reduced and water temperature changes associated with agitation are more easily avoided. 20 mL aliquots of 1 ppm N_2O in N_2 were added to 140 mL syringes. 120 mL degassed nanopure water was added to the syringe, which was vigorously shaken for two minutes. Syringes (in duplicate) were left undisturbed for periods of 0, 12, 30, 56, 92, 121, and 179 minutes after the two minutes of shaking. At the end of the equilibration period, a 5 mL aliquot of headspace was analyzed on the GC. There were no significant differences between peak areas of test samples analyzed immediately after two minutes of shaking (0 minutes) and peak areas of test samples that were left undisturbed for the six longer equilibration periods (Table 1.3, Student's t-test, $p > 0.05$).

Recovery in ISHE

Recovery of N_2O via the ISHE method refers to the quantity of N_2O that is partitioned between the headspace and water with respect to a known initial quantity of N_2O in the 20 mL headspace after equilibration. Testing this recovery helps ensure that the sample has been properly equilibrated prior to analysis. After test samples had been analyzed, excess headspace was expelled from the syringes so that 120 mL equilibrated sample water remained. 20 mL UHP N_2 was then added to each syringe, which were shaken for two minutes to equilibrate the 120 mL water (equilibrated with 20 mL 1 ppm N_2O headspace in previous step) and left undisturbed for periods of 0, 12, 53, 90, and 118 minutes. Headspace was then analyzed in the same manner

as in the previous step. Means of peak areas from the *Testing equilibration time* step samples analyzed immediately after two minutes of shaking (i.e. 0 minutes additional equilibration time) were compared to peak area means generated from the samples that were re-equilibrated with 20 mL UHP N_2 described in this section. There were no significant differences between means in any comparison (Table 1.4, Student's t-test, $p > 0.05$). The purpose of this step was to calculate the percent recovery of N_2O through a mass-balance approach of the moles of N_2O partitioned between the headspace and water in each step. However, no results are given because these tests were run before the GC was operating with optimal sensitivity and precision, and will be repeated in future work under optimal GC performance to confirm N_2O recovery with the ISHE technique and standards of known concentration.

Equilibration temperature

A necessary component of quantifying nitrous oxide (Equation 1) is the temperature of water at the time of equilibration with N_2 headspace, as water temperature affects gas solubility and thus the amount of N_2O that can be dissolved in water**.** Samples preserved using the $HgCl_2$ method are equilibrated at room temperature prior to analysis and that temperature is used to determine the solubility of N_2O in those conditions. Samples collected via the ISHE technique are equilibrated in the field under uncontrolled and varying temperature conditions. It is important to quantify the temperature of the water during field equilibration in order to accurate calculate nitrous oxide solubility. We hypothesized that once the sample is in the syringe, it may warm up or cool down, depending on the air temperature at the field site on any given day and if the scientist holds their hands directly around the syringe

during shaking. Therefore, more accurate temperature measurements than just the *in situ* sample water temperature are required. Thermal exchange during the physical shaking of the syringe may also contribute to water temperature change, but cannot be accurately quantified for the purpose of this study. To understand the in field effect that a two-minute shaking period has on the temperature of the sample water in the field, post-equilibration water temperatures were recorded immediately following the two-minute shaking and headspace extraction using the ISHE technique. This equilibration temperature was then used to calculate N_2O solubility and concentration (Equation 1). Water temperatures increased an average of 1.68˚C˚ from *in situ* temperatures (range = 25.9-32.3˚C, n=134) after the two-minute shaking period based on pre and post shaking water temperatures that were recorded in the field. These post-shaking equilibration temperatures were not significantly different than *in situ* temperatures (Student's t-test, $p < 2.2x10^{-16}$) (Figure 1.6). N_2O concentrations decreased by an average of 3.2% in samples that were above the LOQ after the post-shaking temperature was applied. This change is to be expected, as an increase in water temperature before and after shaking decreases N_2O solubility in water, resulting in lower concentrations. For example, if a sample is calculated to have a N_2O concentration of 10.0 nM based on an *in situ* water temperature of 30.7°C, but water temperature increases by 5°C during the two-minute equilibration period, the calculated N_2O concentration would drop to 9.0 nM due to a decrease in N_2O solubility associated with the increased water temperature. It is important to recognize this sensitivity to temperature change as accurate and precise water temperatures are necessary to correctly calculate N_2O concentrations in a water sample.

Additional in lab experiments were conducted in temperature-controlled rooms at Chesapeake Biological Laboratory to further test the effect that a two-minute shaking period has on the equilibration temperature of the sample water and headspace. Air temperatures were recorded at 1.0, 3.4, 11.0, 14.6, and 20.0°C and water temperatures were allowed to equilibrate before shaking to simulate water conditions colder than those observed in the field tests described above. Water temperatures increased by an average of 2.5˚C and 0.2˚C after the two-minute shake in the 1˚C and 20˚C rooms, respectively (Figure 1.7). Pre and post shaking temperature means differed significantly for each of the five temperature conditions (Student's t-test, $p < 0.05$). Differences in N_2O concentrations were not evaluated in these experiments. These tests demonstrate the importance of recording the water temperature post-equilibration with the use of reliable, calibrated thermometer/probe, in order to accurately quantify N_2O, especially in colder sampling conditions where temperature increases may be more substantial. The results also indicate that care should be taken to minimize the exposure of sample water to highly variable temperatures during sampling and equilibration.

Comparison of ISHE with $HgCl_2$ preservation method

We statistically compared the computed N_2O concentrations from ISHE and $HgCl_2$ treated samples to ascertain where the two methods yielded different results. N_2O concentrations from the $HgCl_2$ method ranged from a minimum of 0.1 nM in July Patuxent River Station 4 bottom waters to a maximum of 19.2 nM in March CBL surface waters. ISHE samples yielded concentrations of 1.2 nM and 19.2 nM for the same respective samples. In general, N_2O concentrations above the LOQ (0.3 ppm)

and atmospheric equilibrium from the ISHE method were in agreement with the $HgCl_2$ method (Figure 1.8). There were no significant differences in sample means between ISHE and $HgCl_2$ preserved samples in 11 of the 20 comparison samples (Table 1.5) (Student's t-test, $p < 0.05$). Seven of the nine significantly different comparisons were below the LOQ (Student's t-test, $p < 0.05$). The significant difference of the two comparison samples above the LOQ may be the result of processing limitations at the time of sampling. Samples from the Patuxent River cruise were not preserved with $HgCl_2$ until 45-60 minutes after sample water collection due to space limitations on the research vessel and associated safety precautions. The 10 mL UHP N_2 headspace exchange was conducted shortly after sample collection. It is possible that a combination of microbial activity in the hour before preservation coupled with temperature changes to the water and headspace during this period may be contributing to the discrepancies of the $HgCl_2$ preserved samples and the ISHE samples.

Percent difference between the ISHE and $HgCl_2$ methods was calculated as follows:

$$\text{ISHE \% above } HgCl_2 = \frac{N_2O \text{ from ISHE } (nM)}{N_2O \text{ from } HgCl_2 \ (nM)} \times 100 \quad (4)$$

Samples collected via the ISHE technique with N_2O concentrations above atmospheric equilibrium had high percent yield with respect to $HgCl_2$ comparison samples (Table 1.5).

The average percent difference between the ISHE and $HgCl_2$ preserved

samples collected from the CBL Pier was found to be 0.05%. The CBL Pier samples were preserved with $HgCl_2$ almost immediately following sample water collection (<5 minutes). The addition of $HgCl_2$ to these samples, coupled with N_2O concentrations higher than atmospheric equilibrium demonstrate the viability of the ISHE technique when compared to $HgCl_2$ preserved samples that have $HgCl_2$ injected in a timely manner. Variability in N_2O concentrations below atmospheric saturation from ISHE samples and $HgCl_2$ may also be the result of detection limitations at low N_2O concentrations. The 27% variability in trace N_2O measurements between the laboratories that participated in the Wilson et al., (2018) intercomparison study supports this idea. To further elucidate the discrepancies between Patuxent River ISHE and $HgCl_2$ comparisons, the addition of a standard lower than 0.3 ppm to the daily calibration curve may help to better evaluate N_2O samples with concentrations at or near atmospheric equilibrium and the current LOQ.

Discussion

Although the $HgCl_2$ method of preserving samples for N_2O analysis is widely used (e.g. Wilson et al., 2018), it is labor intensive and requires the transport, use, and storage of a dangerous anti-biological agent ($HgCl_2$). The ISHE method described in this chapter alleviates the use of caustic chemicals, lowers overall waste disposal costs, and is it efficient to conduct in the field (<10 minutes for extraction). From the samples collected and analyzed in this study that were above the LOQ, we find that N_2O concentrations from ISHE samples average ±2.5% of those collected with $HgCl_2$ preservation, which is within the acceptable range of variance. These N_2O concentrations ranged from 6.8-19.2nM N_2O and were across a salinity range of 0.2-

8.7 and water temperature range of 8.1-29.1°C. Wilson et al. (2018) reports coefficients of variance between 2.8-7.5% for the N_2O samples analyzed in their intercomparison study. The mean coefficients of variance for ISHE samples and $HgCl_2$ preserved samples above the LOQ were 2.9% and 2.1%, respectively, demonstrating that the variability between samples is comparable, and in some cases lower than the variability reported by Wilson et al. (2018).

While the variance in our study fits within acceptable ranges, it is still worthwhile to consider some of the discrepancies in N_2O concentrations of the $HgCl_2$ preserved samples and the ISHE method samples. These could be the result of the temperature sensitivity of the ISHE method during the equilibration period. Because the water temperature at the time of headspace equilibration alters the solubility of N_2O, it is important to properly denote that water temperature after the two-minute shaking of the ISHE syringe. While effort was taken in the field to properly record the final temperature of the water after the two-minute equilibration period, there may be more effective ways to do so. The use of a more sensitive thermometer in the field could help address some of the differences in the ISHE and $HgCl_2$ collected samples in the future. Due to the effect that equilibration temperature has on N_2O solubility, it may be that the differences between the samples are a product of temperature error, and can be corrected.

Given the ubiquity of using $HgCl_2$ to preserve water samples for N_2O analysis, there is an absence of literature that discusses the analytical testing of the $HgCl_2$ method that would justify its designation as the benchmark approach for N_2O sample collection. The use of $HgCl_2$ follows a widespread convention of using the

chemical as a biological arresting agent in samples for a wide diversity of solutes and gases. Without a standardized method paper to prove the precision and accuracy of the $HgCl_2$ technique, it is worth considering if $HgCl_2$ addition is a necessary method for sample preservation. The comparison of $HgCl_2$ preserved samples to those with no preservation presented by Yoshinari (1976) suggests that the use of $HgCl_2$ may not be required under most conditions. It is possible that the unpreserved samples from the Yoshinari (1976) study diverged from the $HgCl_2$ preserved samples because biological activity altered N_2O levels in the sample water during the month prior to analysis. If un-treated samples were measured within 24 hours of collection, biological activity might not have enough time to measurably alter N_2O concentrations. Further analysis is needed to understand an acceptable sample storage time that ensures stability in N_2O concentrations.

The ISHE technique presented in this paper is unique in that it eliminates the need to preserve sample water by equilibrating and extracting headspace in the field, removing the possibility for biological activity to affect N_2O levels between sampling and analysis. This procedure provides a safer alternative to the $HgCl_2$ method, especially in waters that are likely to have elevated N_2O concentrations with respect to atmospheric equilibrium due to high nutrient loads and oxic conditions that facilitate N_2O production. With a growing interest in quantifying N_2O concentrations to better understand distributions and air-sea fluxes in coastal and estuarine systems, and the contribution of these systems to the global N_2O budget, the ISHE technique presented here provides a safe, cheap, and efficient alternative to traditional methods while also meeting acceptable standards for variance between replicate samples.

Future laboratory tests

Although the data presented in this study demonstrate the practicality of the ISHE technique in waters with N_2O concentrations above atmospheric equilibrium, additional testing is necessary to further establish its viability, especially in systems that contain low concentrations of N_2O. Analytical precision of the method at lower N_2O concentrations may be further increased with a more extensive daily calibration curve that incorporates standards below 0.3 ppm. The calibration standards used in this study were created by diluting a 1 ppm N_2O in N_2 certified standard with UHP N_2 to achieve the desired partial pressures for the 5-point calibration curve. A more representative standard curve may be established by creating the standards and extracting them in the same manner as ISHE samples. This will also allow for the calculation of the % recovery of N_2O with the ISHE method to ensure that the amount of N_2O (in moles) that is theoretically partitioned between the headspace and water can be accounted for following analysis of the headspace on the GC.

Further testing of ISHE robustness will include equilibrating degassed nanopure water with a known concentration of N_2O headspace, spiking with $HgCl_2$, and analyzing the equilibrated headspace with GC-ECD. ISHE samples will be processed in the same manner described above, and resulting N_2O concentrations of the $HgCl_2$ preserved and ISHE test samples will be compared. This test will occur with varying known concentrations of N_2O to better establish the LOQ (and potential LOD) for the ISHE technique.

Application of ISHE – Chesapeake Bay wide sampling

A primary motivation behind the development of the ISHE technique as an

alternative to the standard $HgCl_2$ method was to eliminate the use of a toxic preservative and allow for safer and more convenient collection of samples to be analyzed for N_2O. As demonstrated in this study, the ISHE technique serves as an alternative in systems likely to experience elevated N_2O concentrations. Using the ISHE technique, samples spanning a large portion of the main stem Chesapeake Bay were collected and analyzed N_2O to better understand Chesapeake Bay-wide spatial N_2O distributions (Figure 1.9). In all sampling locations, N_2O was above atmospheric equilibrium and there were high concentrations of N_2O in shallow, eutrophic tributaries relative to the open, more saline waters of the mainstem of Chesapeake Bay (Figure 1.9). Given the pervasive condition of elevated N_2O concentrations relative to atmospheric equilibrium throughout Chesapeake Bay, the estuary appears to be a source of N_2O to the atmosphere. The ISHE technique provides an efficient and safe method to help close the knowledge gap regarding controls, distributions, and air-sea flux of N_2O from anthropogenically influenced systems such as Chesapeake Bay, and may help better constrain the contribution of estuaries to the global N_2O budget.

Tables

Table 1.1 SRI Instruments Gas Chromatograph with Electron Capture Detector settings used in this study.

Category	Setting
Column Oven Temperature	100˚C
ECD Current	900 mV
N_2 flow	26 psi
Run Time	10 minutes

Table 1.2 Comparison of intercalibration standard (326.5 ppb) to calculated concentration from daily standard curves.

Analysis Date	Calculated concentration from daily standard curve (ppb)	Offset from reported concentration (326.5 ppb)
8/1/2019	326.1	-0.1%
8/5/2019	343.6	5.2%
8/7/2019	343.1	5.1%
Average	337.6	3.4%

Table 1.3 Means comparison of peak areas from samples equilibrated for various times after two-minute equilibration period. No significant differences were observed between the shortest equilibration time and longer periods ($p>0.05$).

Equilibration time comparison after two-minute shaking period (minutes)	Average area of N_2O peaks for equilibration time comparisons	Student's t-test *p* value
0 vs. 12	26.43 vs. 28.77	0.35
0 vs. 30	26.43 vs. 26.35	0.96
0 vs. 56	26.43 vs. 26.48	0.96
0 vs. 92	26.43 vs. 24.76	0.21
0 vs. 121	26.43 vs. 28.84	0.12
0 vs. 179	26.43 vs. 28.63	0.26

Table 1.4 Means comparison of peak areas from *Testing equilibration time* test samples versus *Recovery in ISHE* test samples of varying post-shaking equilibration times. No significant differences were observed ($p>0.05$).

Equilibration time after two-minute shaking period of test samples (minutes)	Average area of N_2O peaks for equilibration time comparisons	Student's t-test *p* value
0 vs. 12	26.43 vs. 22.20	0.27
0 vs. 53	26.43 vs. 20.20	0.17
0 vs. 90	26.43 vs. 21.78	0.10
0 vs. 118	26.43 vs. 25.10	0.77

Table 1.5 Means comparison and N_2O concentrations from ISHE and $HgCl_2$ preserved samples (nM ± SD). Means that are not significantly different denoted by * ($p > 0.05$). Concentrations in red are below the Limit of Quantitation.

Sample ID	Student's t-test *p* value	N_2O (nM) ISHE	N_2O (nM) $HgCl_2$	Concentration Difference (ISHE - $HgCl_2$) (nM)	ISHE % above $HgCl_2$
CBL (Surface March)	0.119*	19.7 ± 0.9	18.4 ± 0.1	1.4	7%
CBL (Bottom March)	0.858*	19.2 ± 0.9	19.2 ± 0.7	0.1	0%
CBL (Surface June)	0.076*	13.3 ± 0.2	13.7 ± 0.9	-0.4	-3%
CBL (Bottom June)	0.118*	14.5 ± 0.3	15.0 ± 0.2	-0.5	-3%
CBL (Surface June)	1*	11.2 ± 0.1	11.2 ± 0.3	0.0	0%
CBL (Bottom June)	0.541*	11.6 ± 0.3	11.8 ± 0.4	-0.2	-2%
PAX S1 (0.7m)	0.011	9.6 ± 0.3	11.7 ± 0.3	-2.1	-18%
PAX S1 (1.6m)	0.000	10.4 ± 0.1	12.3 0.03	-1.9	-16%
PAX S2 (0.7m)	0.020	7.8 ± 0.3	6.4 ± 0.3	1.4	21%
PAX S2 (2.4m)	0.034	7.6 ± 0.3	6.8 ± 0.02	0.8	12%
PAX S3 (0.9m)	0.798*	5.7 ± 0.3	5.6 ± 0.7	0.1	2%
PAX S3 (2.0m)	0.051*	5.2 ± 0.2	4.3 ± 0.3	0.9	22%
PAX S3 (3.9m)	0.029	2.8 ± 0.2	1.6 ± 0.1	1.2	76%
PAX S3 (7.9m)	0.002	1.6 ± 0.1	0.2 ± 0.004	1.4	623%
PAX S3 (10.4m)	0.001	1.6 ± 0.1	0.2 ± 0.01	1.4	660%
PAX S4 (0.9m)	0.023	6.4 ± 0.3	5.3 ± 0.2	1.0	19%
PAX S4 (3.3m)	0.002	6.1 ± 0.1	5.4 ± 0.2	0.7	12%
PAX S4 (5.4m)	0.088*	5.7 ± 0.8	4.4 ± 0.1	1.3	31%
PAX S4 (8.2m)	0.264*	4.4 ± 0.7	3.2 ± 0.05	1.2	39%
PAX S4 (15.9)	0.293*	1.2 ± 0.8	0.1 ± 0.1	1.1	921%

Figures

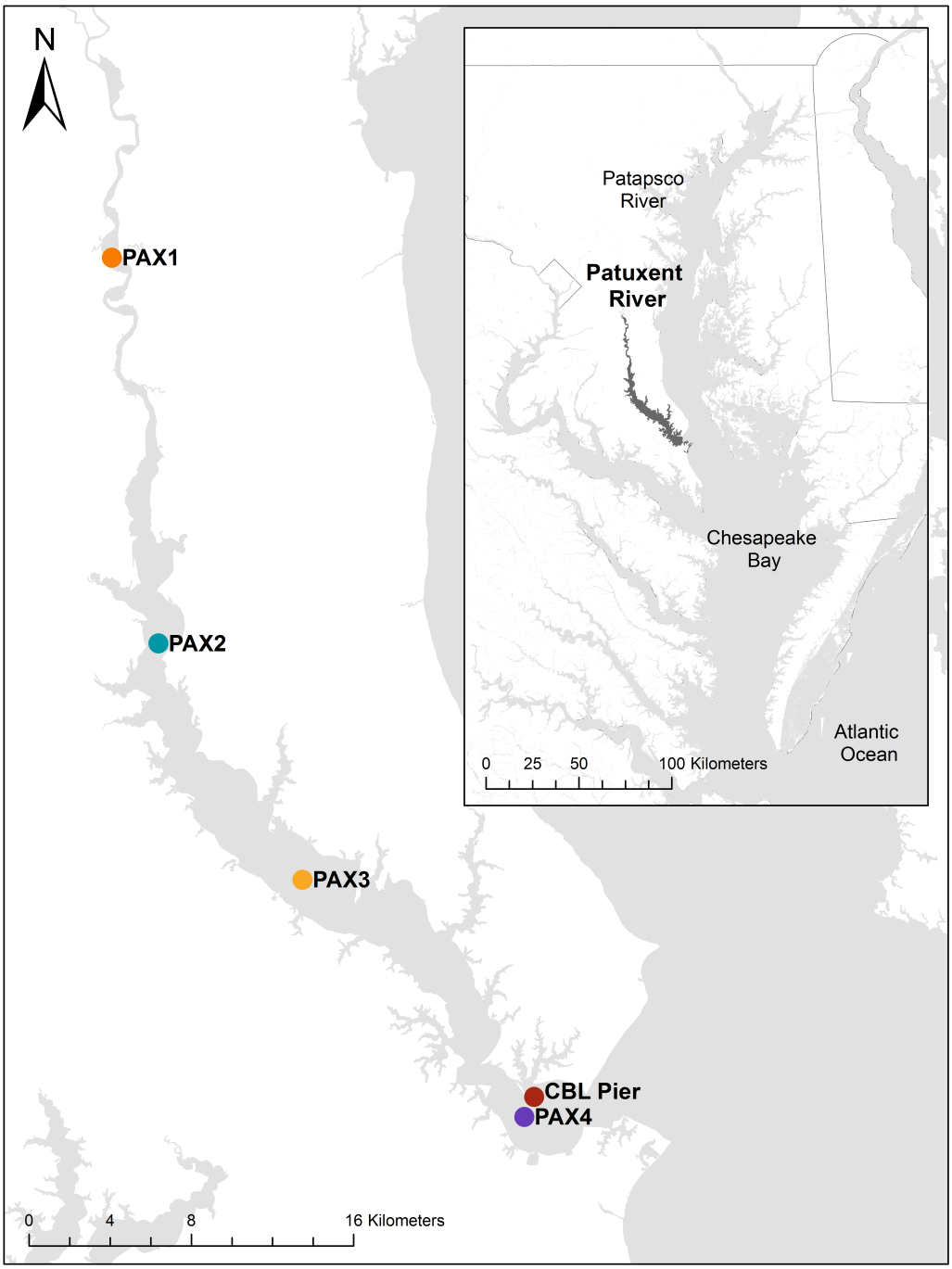

Figure 1.1 Map of the Patuxent River estuary within the context of Chesapeake Bay (see inset). Patuxent River stations and Chesapeake Biological Laboratory Research Pier denoted by colored circles.

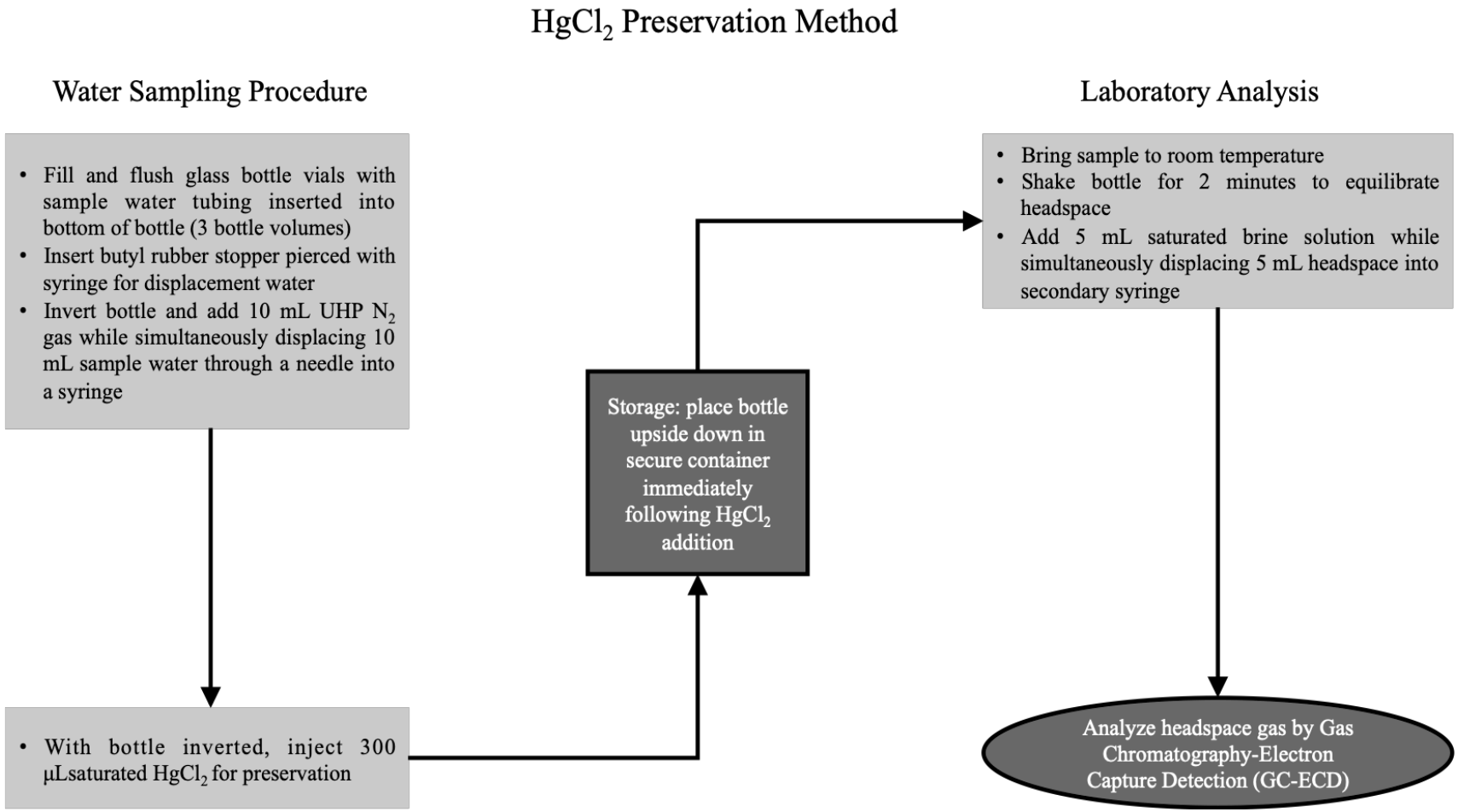

Figure 1.2 Flow chart of sampling sequence events and laboratory analysis using the $HgCl_2$ preservation method.

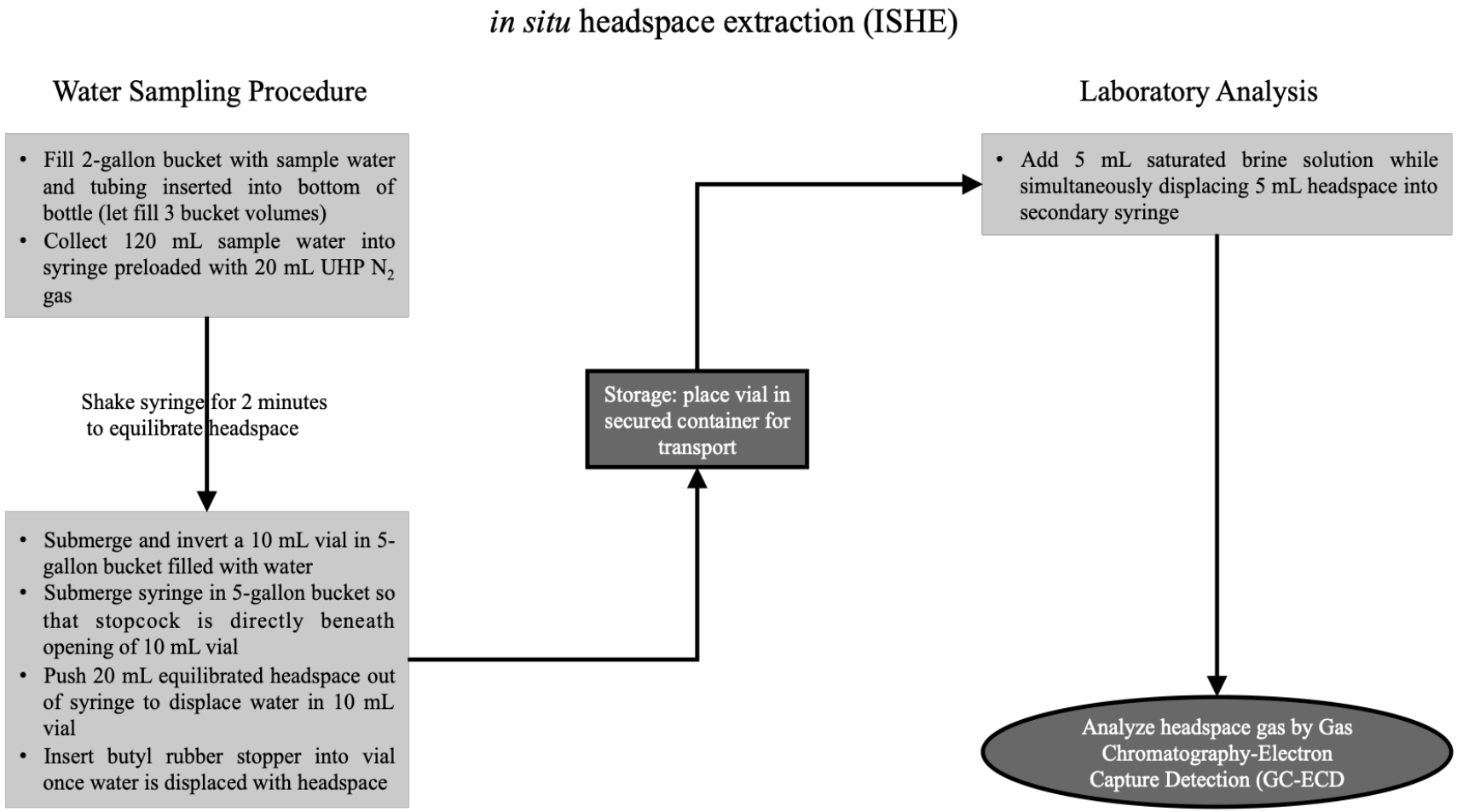

Figure 1.3 Flow chart of sampling sequence events and laboratory analysis using the ISHE technique.

Figure 1.4 (a) Syringe and glass serum vials used for ISHE technique, (b) headspace extraction from 140 mL syringe to 10 mL vial, and (c) size comparison of ISHE vial (left) and $HgCl_2$ bottle (right) after headspace exchange.

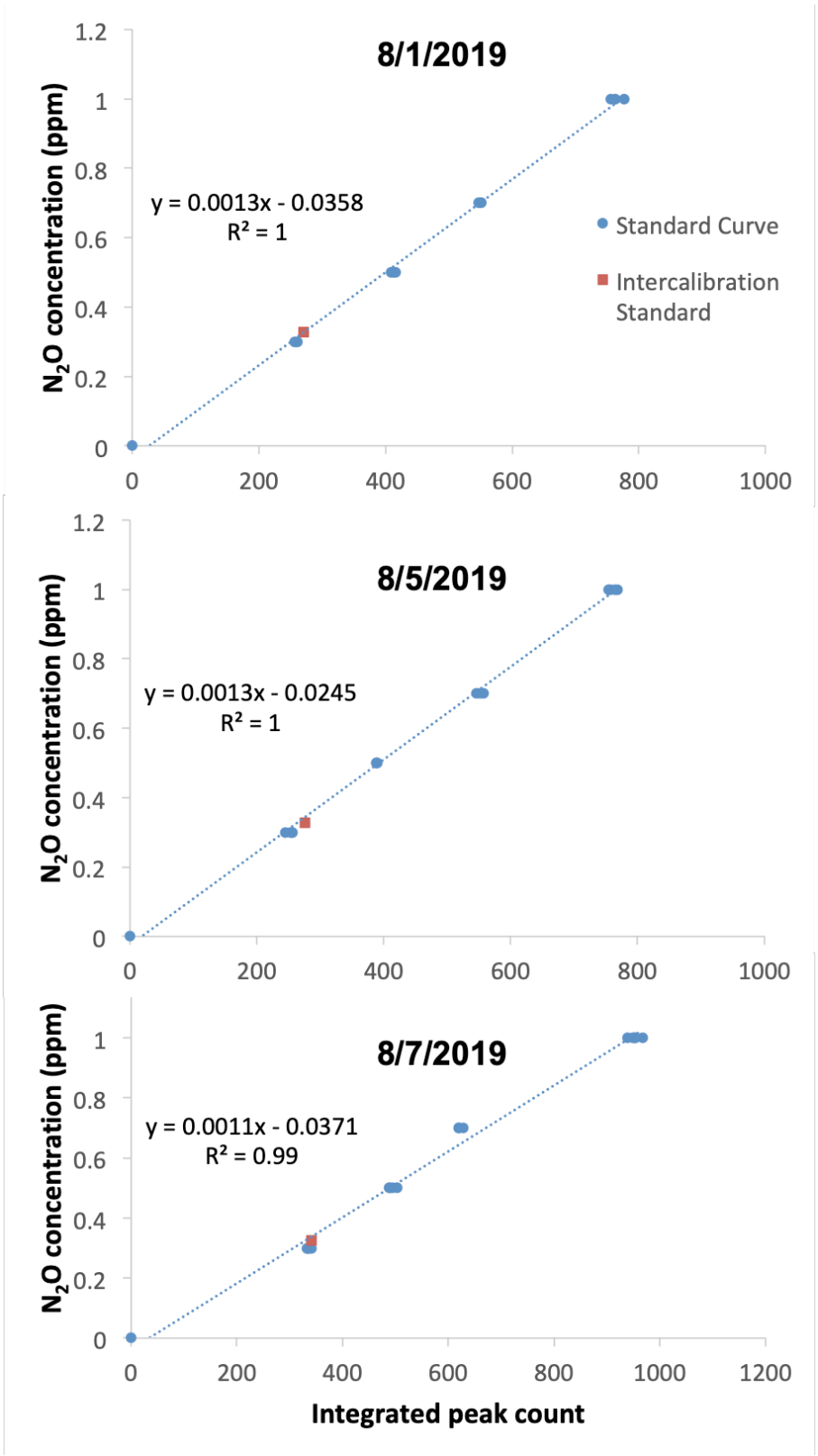

Figure 1.5 Standard curves from three days that the intercalibration standard was analyzed. Red square represents triplicate runs of intercalibration standard. Average offset of intercalibration standard concentration calculated from daily standard curves is 3.4% from reported concentration of 326.5 ppb.

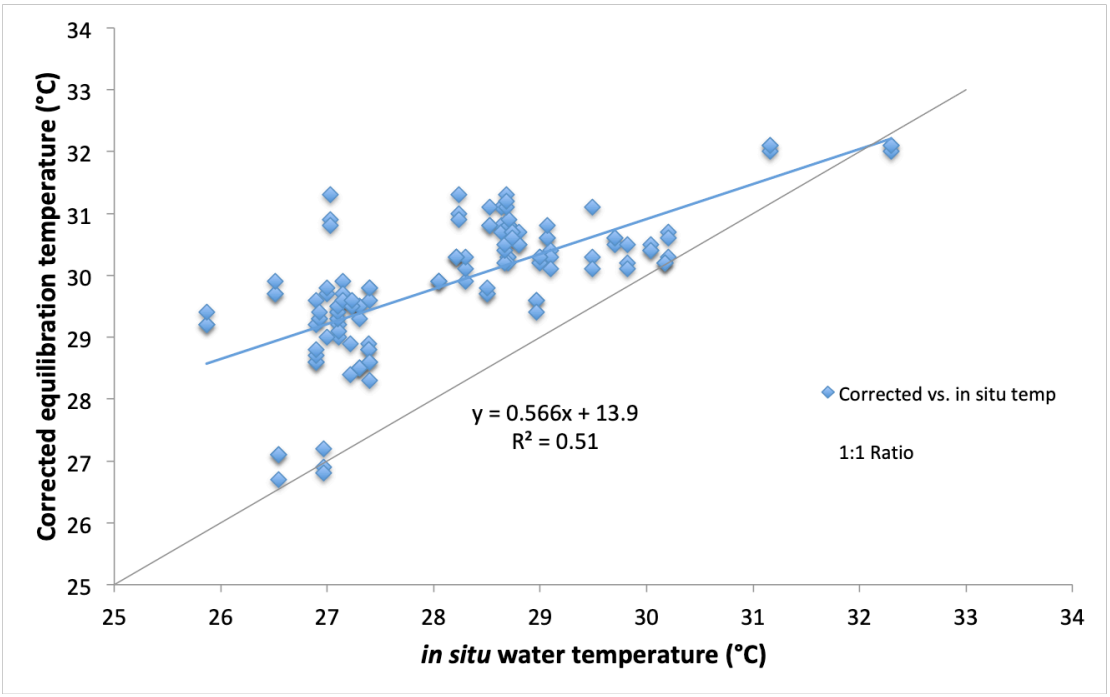

Figure 1.6 Correlation between corrected equilibration temperature and *in situ* field recorded water temperature. Corrected equilibration temperature recorded after two-minute shaking period of 140 mL used in ISHE method. Results demonstrate an increase in water temperature after the two-minute equilibration period.

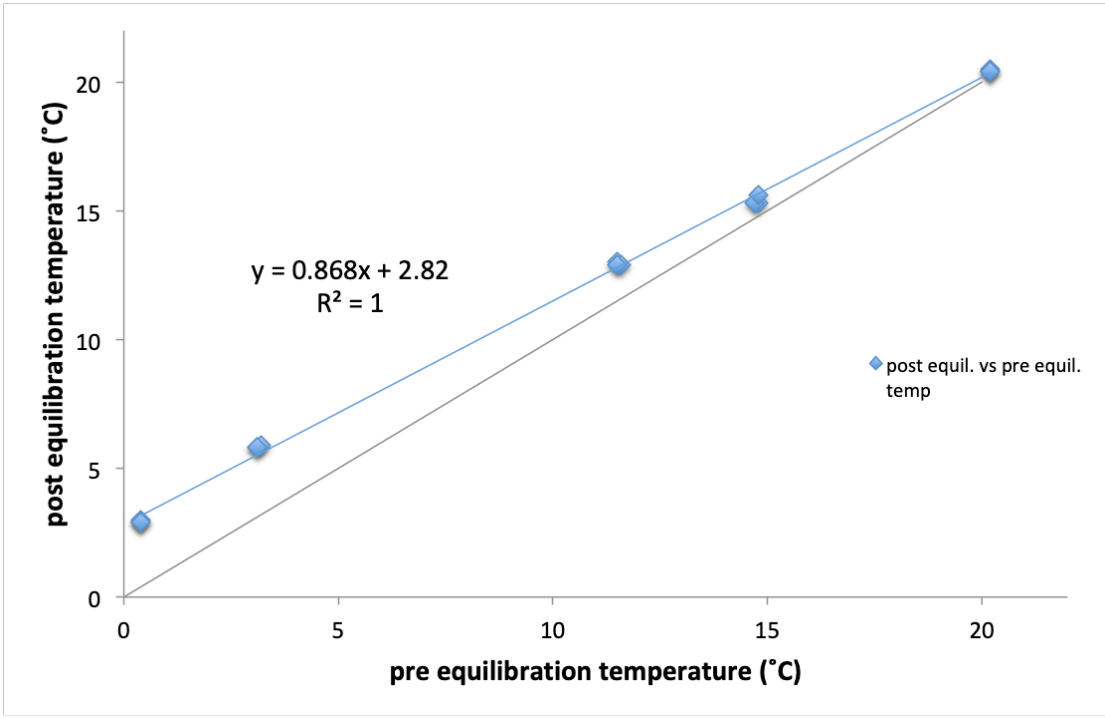

Figure 1.7 Relationship between post equilibration and initial water temperature in 140 mL syringes used for ISHE method. Tests were conducted in temperature-controlled rooms at Chesapeake Biological Laboratory.

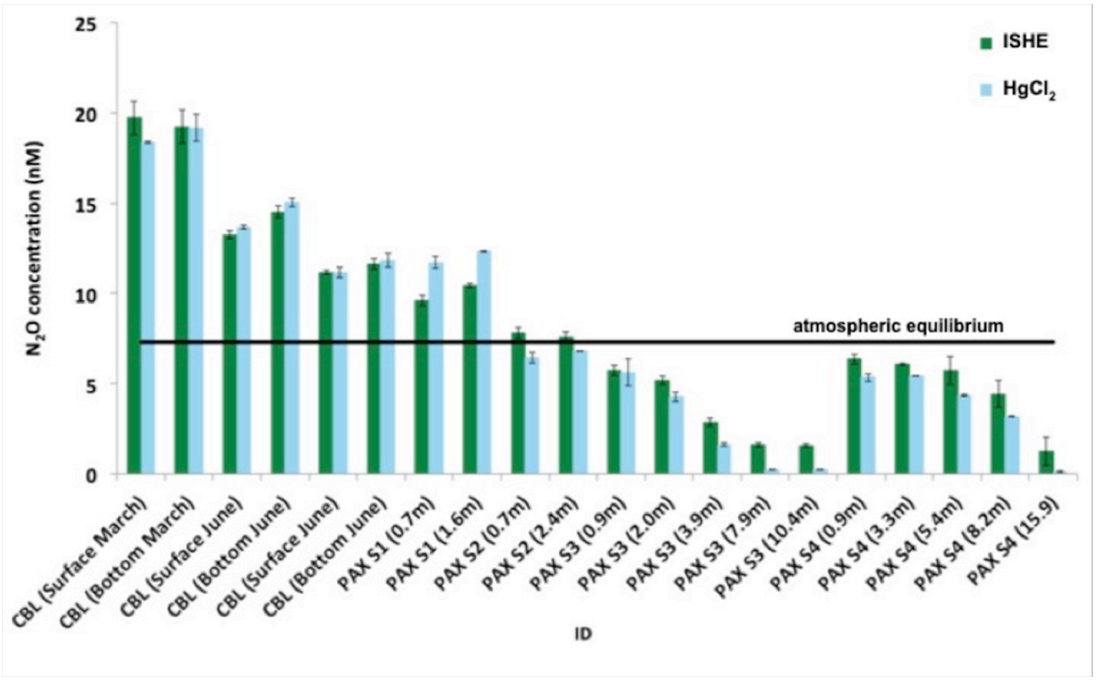

Figure 1.8 Comparison of ISHE and $HgCl_2$ sampling techniques. Graphic representation of Table 5. Results demonstrate viability of ISHE as alternative method. Samples were collected from surface and bottom waters off the Chesapeake Biological Laboratory monitoring pier once in March 2019 and twice in July 2019 and at multiple depths at four stations spanning the salinity gradient of the Patuxent River. Error bars represent standard deviation of triplicate samples.

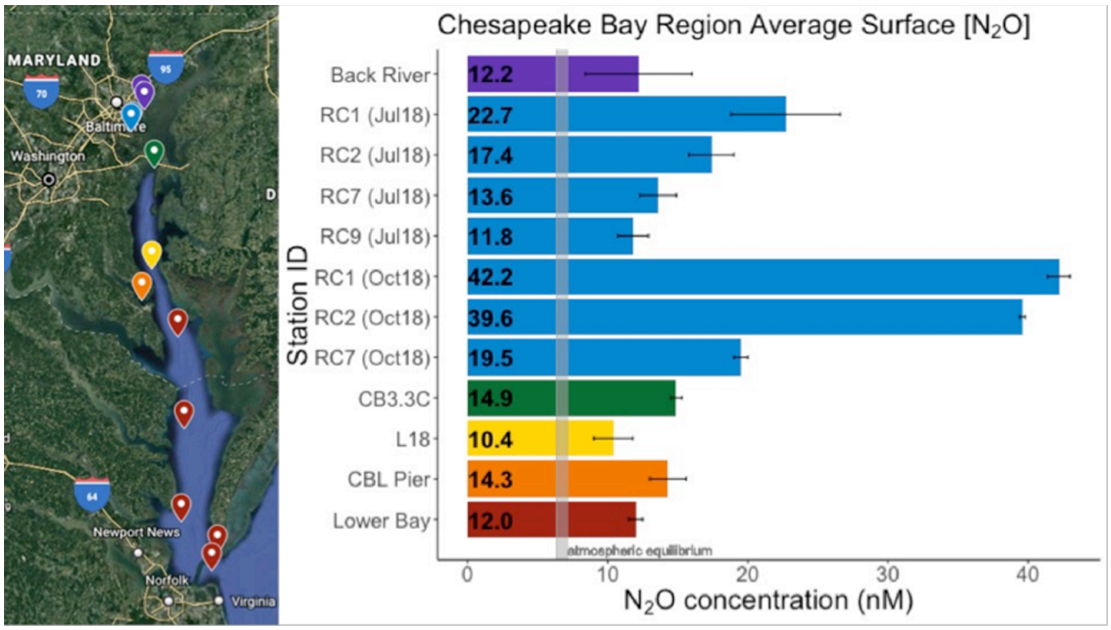

Figure 1.9 Surface water N_2O concentrations (nM) from Chesapeake Bay region locations samples using ISHE technique. L18 station data from Laperriere et al. (2018).

Chapter 2

Introduction

Nitrous oxide (N_2O) is a common dissolved gas in freshwater and estuarine environments that has a greenhouse potential ~300 times greater than carbon dioxide (IPCC, 2007). Atmospheric N_2O concentrations have increased significantly since preindustrial times and have been projected to continue to rise with further human activity (Bange et al., 1996; IPCC, 2013). Emissions from anthropogenic activities such as agricultural practices, power plant operations, motor vehicle emissions, and wastewater treatment plants (WWTPs) contribute to the global N_2O increase (Becker et al., 1999; Dones et al., 2004; Galloway et al., 1995; Mosier et al., 1998; Parravicini et al., 2016). Nitrous oxide is also naturally produced in coastal and marine environments as a byproduct of biogeochemical nitrogen cycling (de Wilde and de Bie, 2000; Ji et al, 2015; Upstill-Goddard, 2011). Naturally produced N_2O is estimated to account for 60-70% of the ~17 Tg N_2O emitted each year (Wuebbles, 2009), 0.31 Tg N_2O yr^{-1} of which is generated by estuarine ecosystems (Murray et al., 2015). Recent interest in N_2O has led to advances in our understanding of controlling mechanisms in marine waters, where high N_2O production rates and concentrations have been measured in the suboxic zones of the open ocean (Babbin et al., 2015; Bange et al., 2001; Yoshinari et al., 1997) and in highly eutrophic low salinity waters (e.g. Cole and Caraco 2001; Garnier et al., 2006; Rajkumar et al. 2008). Despite these prior studies and the importance of this gas for understanding the generation of

greenhouse gas emissions, there is still a knowledge gap regarding N_2O controls and distributions in estuarine and coastal waters.

Nitrous oxide is produced and consumed by a variety of processes within the nitrogen cycle. The coupled, microbially mediated biogeochemical processes within the nitrogen cycle responsible for nitrous oxide generation and consumption are nitrification and denitrification. Nitrification is an aerobic process by which ammonia (NH_3) is oxidized to nitrite (NO_2^-) and ultimately to nitrate (NO_3^-), and serves as a production pathway for N_2O (Barnes and Upstill-Goddard, 2011; de Wilde and de Bie, 2000; Ji et al., 2015, Nevison et al., 2003). Nitrous oxide is generated specifically during the oxidation of the intermediate species hydroxylamine (NH_2OH) to nitric oxide (NO^-) during nitrification (Korth et al., 2019; Zhu et al., 2013). Denitrification is an anaerobic process that reduces NO_3^- to NO_2^-, NO^-, N_2O, and N_2 gas (Figure 2.1) and can be inhibited by the presence of oxygen (Oh and Silverstein, 1999; Von Schulthess et al., 1994). Nitrous oxide is produced and then consumed during this stepwise reduction of nitrate to N_2 and acts as the terminal electron acceptor in the final step of the process. However, nitrous oxide reductase, the key enzyme that catalyzes the conversion of N_2O to N_2 in denitrification is inhibited by oxygen. This inhibition of the final step of denitrification can result in an incompletion of the process and N_2O generation rather than consumption (Hanaki and Matsuo, 1992; Ligi et al., 2013; Otte et al., 1996; Palta et al., 2013; Quick et al., 2019; Tiedje, 1988).

Other aspects of the nitrogen cycle can indirectly contribute to N_2O dynamics. Dissimilatory nitrate reduction to ammonium (DNRA), can potentially generate N_2O,

but its contribution to global N_2O production is not as well studied as nitrification and denitrification (Quick et al., 2019). DNRA is a process by which NO_3^- is first reduced to NO_2^- and then to NH_4^+ (Lansdown et al., 2012; Smith, 1982; Sun et al., 2018). Unlike denitrification, N_2O is not produced as an intermediate species during DNRA, but instead is generated only when NO_2^- accumulates and biotic and abiotic pathways reduce it to N_2O. As such, DNRA can compete with denitrification for NO_3^-, potentially inhibiting N_2O production from denitrification if DNRA goes to completion (Quick et al., 2019). Anaerobic ammonium oxidation (anammox) is another process in the nitrogen cycle that has been considered as a potential N_2O production pathway, but its contribution to N_2O generation has been demonstrated to be trivial (Hu et al., 2015; Stein and Yung, 2003). At no point during anammox is N_2O produced as an intermediate and similar to DNRA, anammox may limit N_2O production by competing with denitrification for NO_2^-, which is used to oxidize NH_4^+ to N_2 in the anammox process (Quick et al., 2019).

N_2O tends to reach peak concentrations in regions where either high ammonium inputs and concentrations or opposing oxygen and ammonium gradients allow for high rates of nitrification, including the sub-oxic zones of the Pacific, the Chesapeake Bay pycnocline, and tidal freshwater regions like the Hudson River (Cole and Caraco 2001; Garnier et al. 2006; Ji et al., 2015; LaPierre et al., 2018; Santoro et al., 2011). In contrast, N_2O reaches minima where production rates are low or denitrification consumes N_2O. In polluted estuaries such as Chesapeake Bay and its shallow, anthropogenically influenced tributaries, nitrous oxide levels are likely to be elevated, but dynamic physical and chemical environments can lead to highly variable

N_2O concentrations. Where eutrophication occurs, high nutrient variability and strong gradients of oxygenation can alter nitrogen cycling rates and affect N_2O production, such as stimulating nitrification in ammonium rich waters or encouraging denitrification in anoxic sediments. N_2O concentrations are high in polluted upper reaches of rivers, where high ammonium oxidation rates lead to high rates of N_2O production (e.g., Garnier et al. 2006). Controlled ecosystem eutrophication experiments have shown that N_2O production in sediments is non-linearly elevated along a gradient of increasing nutrient loading (Seitzinger et al., 1980). Although eutrophication can stimulate N_2O production through high nitrification rates, if that eutrophication stimulates anoxia and sulfide production, nitrification can be inhibited (Joye and Hollibaugh, 1995). Given these dynamic estuarine processes and their direct and indirect impacts on N_2O, accurately quantifying nitrous oxide in estuarine waters is necessary to broaden our understanding of N_2O cycling, air-water flux, and distribution within estuarine and coastal ecosystems.

The objectives of this study were to quantify the spatial and temporal distributions of nitrous oxide concentrations and fluxes in three tidal tributaries of a eutrophic estuary (Patapsco River, Maryland, USA) in times of varying oxygen and nutrient conditions to better understand the controls and distributions of N_2O in eutrophic waters. In particular, we sought to investigate the influence that oxygen and nutrient ability have on the generation of N_2O during coupled nitrification-denitrification. To accomplish this, we performed a comparative, cross-system analysis to understand the impacts of engineered aeration on nitrogen cycling and N_2O availability. This effort included experiments where deoxygenation and

reoxygenation were artificially induced by manipulation of an aeration system in Rock Creek, a tributary of the Patapsco River.

Methods

Study area

The Patapsco River (MD) is a Chesapeake Bay tributary located south of Baltimore, Maryland, USA that has high rates of nitrogen loading and is highly impaired (Sellner et al., 2001). Stoney Creek, Rock Creek, and Bodkin Creek are three adjacent tidal sub-tributaries to Patapsco River located within a broader, anthropogenically-influenced watershed (Figure 2.2). Urban development contributes to high nutrient loads that can facilitate eutrophication and sub-oxic conditions in these systems. Rock Creek in particular has experienced historically poor water quality resulting in seasonal anoxia, fish kills, and hydrogen sulfide (H_2S) release from sediments in warmer months (Harris et al, 2015). In 1988 an ecological engineered practice (EEP) was installed in the creek to help mitigate the poor water quality conditions. This EEP is in the form of a large-scale aeration system and acts to de-stratify and oxygenate the water column to alleviate sub-oxic conditions and mitigate the repercussions associated with sub-oxic waters that facilitate fish kills and foul odors from H_2S release in warmer months. Recent studies conducted within Rock Creek have experimentally deoxygenated the estuary in order to quantify how oxygen depletion alters water column nutrient concentrations, sediment-water nutrient and oxygen fluxes, and denitrification (Harris et al., 2015). Once the aeration system was turned off after bottom waters reached anoxic levels, Harris et al., (2015)

report NO_3^- and NO_2^- uptake, decrease in phosphate fluxes from sediments, and an increase in denitrification rates. The aeration system in Rock Creek makes it highly unique and provides the opportunity to study how engineered oxygenation can affect biogeochemical cycling in polluted waters. In Stoney Creek and Bodkin Creek, which are also tidal tributaries to the Patapsco River immediately adjacent to Rock Creek, similar human-induced deoxygenation problems have not been reported and these tributaries have remained largely unstudied, contrary to Rock Creek. Characteristics of each creek can be found in Table 2.1 The potential for these creeks to experience eutrophic and sub-oxic conditions similar to Rock Creek qualifies them as appropriate comparison sites to study the effects of oxygenation and nutrient loading on nitrous oxide generation in anthropogenically-influenced waters.

A cross-system comparison of Rock Creek to Bodkin Creek and Stoney Creek allows for the study of spatial and temporal distributions of N_2O in three potentially similar systems. The engineered aeration in Rock Creek also provides the ability to specifically investigate how altered oxygenation affects the generation of nitrous oxide in warmer months. These data will help to specifically understand (1) the spatial and temporal N_2O concentrations and distributions in three anthropogenically influenced Patapsco River tributaries, (2) the air-sea flux of N_2O in these creeks relative to similar systems, and (3) the influence of nutrient and oxygen availability on N_2O production in these estuarine systems to provide a broader understanding of controls on nitrous oxide concentrations in coastal and estuarine systems.

Sample Collection

Water and sediment sampling and sediment-water flux measurements were conducted in April and July 2019 in all three creeks to capture seasonal variability in nitrous oxide concentrations, nutrient availability, oxygen conditions, and sediment-water flux rates. All creeks were sampled once in April, and Stoney Creek and Bodkin Creek were sampled once in July, while Rock Creek was sampled twice; once during a period of active aeration and again after two weeks of inactive aeration. Aeration was turned off to allow Rock Creek waters to reach naturally sub-oxic conditions for experimental purposes. Four stations were sampled along the tidal axis of each creek with the most upstream station located near the headwaters and most downstream station towards the mouth of the tributary (Figure 2.2).

At each station, water column hydrocasts were conducted at 0.5m depth intervals to profile physical parameters including temperature, conductivity, salinity, dissolved oxygen (DO), and pH using a YSI EXO 2. Following the hydrocasts, surface and bottom water samples were collected via a submersible bilge pump and processed through 0.7µm GF/F filters for analysis of nitrate+nitrite (NO_{23}^-), nitrite (NO_2^-), ammonium (NH_4^+), particulate nitrogen (PN), total dissolved nitrogen (TDN), chlorophyll a, phaeophytin, and total suspended sediments (TSS). Nutrient samples were later analyzed by the Nutrient Analytical Services Laboratory at Chesapeake Biological Laboratory using standard analytical methods for each variable (https://www.umces.edu/nasl/methods). Nitrous oxide samples were collected in triplicate from surface and bottom waters at all stations via an *in situ* headspace extraction (ISHE) method described in Chapter 1.

Sediment-water fluxes of dissolved nitrogen solutes and gases were measured in the uppermost station of each creek via core incubation experiments during April and July sampling cruises. In the field, duplicate sediment cores were collected using a plexiglass cylinder 6.5 cm in diameter. Intact sediment cores were extracted via a pole coring technique and kept in an ambient water-filled cooler until incubation experiments began. Cores were then flushed with local bottom water collected on station for one hour and incubated at ambient temperatures for three hours following collection. During incubations, water samples for N_2, Ar, NH_4^+, NO_{23}, and NO_2^- were extracted from overlying water within cores every 60 minutes and fixed with 10 µL saturated $HgCl_2$ for preservation. A 'blank' core was also incubated that contained only water to allow for water-column contributions to solute changes to be measured. Following incubations, nitrogen and argon gas concentrations were measured within 28 days (after being kept at ambient temperature) using a Bay Instruments Membrane Inlet Mass Spectrometer (MIMS) (Kana et al., 1994) and NH_4^+, NO_{23}, and NO_2^- were analyzed with the same approach as the overlying water. The resulting time courses of dissolved solutes were fit with linear regressions to compute a slope, which was then corrected for core water volume and area to compute a rate of sediment-water flux. Only fluxes with correlation coefficients exceeding 0.85 were included in later analysis (Pérez-Villalona et al., 2015). An additional sediment core was collected on site and 1 cm of surface sediment was immediately collected, stored on ice, and later analyzed for particulate carbon and particulate nitrogen (PC/PN) using USEPA Method No. 440.0 and chlorophyll a using USEPA Method 446.0 and Standard Methods 10200H.

Analysis Techniques

Samples collected for nitrous oxide measurements were analyzed at the Chesapeake Biological Laboratory using the sample and calibration curve analysis techniques outlined in Chapter 1. A five-point calibration curve was run at the beginning and end of each day using standards of 0, 0.3, 0.5, 0.7, and 1ppm N_2O standards.

Air-sea flux of nitrous oxide was calculated using the following equation:

$$Flux = 0.251u^2 \left(\frac{Sc}{660}\right)^{-0.5} K_O([G_w] - [G_a]) \quad (1)$$

where 0.251 is the optimal gas transfer coefficient in units of (cm hr^{-1}) (m s^{-1})$^{-2}$, u is wind speed in (m s^{-1})^2, Sc is the Schmidt coefficient based on kinematic viscosity of water and the diffusion coefficient of N_2O (Sweeney et al., 2007; Weis, 1970; Weiss and Price, 1980; Wanninkhof, 1992; Wanninkhof, 2014), K_O is a salinity and temperature dependent coefficient in mol L^{-1} atm^{-1}, G_w and G_a are the respective concentrations of N_2O in the water and air in units of atm. The final reported flux is in units of μmol N_2O m^{-2} d^{-1}. Wind speed data was acquired from the National Oceanic and Atmospheric Administration (NOAA) National Data Buoy Center (NDBC) Station BLTM2 - 8574680 and adjusted based on field recorded *in situ* wind speed data recorded on field days. NOAA NDBC data is reported in 6-minute intervals and was averaged for the day of field sampling. The field recorded *in situ* wind speeds were higher than NDBC data by an average of 1.07. This correction coefficient was applied to the NDBC data to normalize the wind speeds used in flux calculations. This wind speed was then normalized to a height of 10m via the following equation (Marino & Howarth, 1993):

$$U10 = \frac{U}{0.097 * \log\left(\frac{H}{10}\right) + 1} \quad (2)$$

where U is the corrected NDBC wind speed (m s^{-1}) and H is the height of the anemometer above water level (m). Flux in is units of mol N_2O m^{-2} yr^{-1} after unit conversions.

Nitrous Oxide Yields and Production Rates

Nitrous oxide yields and production rates in sediments were calculated using four methods. The first calculation is based on SOD (sediment oxygen demand; from sediment cores, µmol O_2 m^{-2} hr^{-1}) for upstream stations in each creek. Nitrogen remineralization rate (µmol N m^{-2} hr^{-1}) was calculated via the following equation:

$$Nitrogen\ remineralization\ rate = SOD\ rate \times \frac{16\ mol\ N}{138\ mol\ O_2} \quad (3)$$

(Takahashi et al., 1985).

N_2O production rate (µmol N m^{-2} d^{-1}) is calculated using the following equation:

$$N_2O\ production\ rate = J_1 + J_2 \quad (4)$$

where J_1 represents aerobic NH_4^+ oxidation to N_2O and J_2 represents N_2O production from NO_3^- and NO_2^- reduction in anaerobic environments. J_1 is calculated via the following equation:

$$J_1 = \left(\frac{a}{[O_2]} + b\right) \times 0.01 \times Nitrogen\ remineralization\ rate \quad (5)$$

Where a and b are coefficients (0.2 μM O_2 and 0.08, respectively) derived from an empirical relationship between N_2O yield from nitrification and O_2 concentrations (Ji et al., 2018). J_2 is calculated via the following equation:

$$J_2 = (\beta \times f(O_2) \times Nitrogen\ remineralization\ rate \quad (6)$$

In which β is a unitless coefficient of 0.215 that represents the increased production of N_2O from denitrification in oxygen limiting environments (Sutharalingam et al., 2012).

$$f(O_2) = \exp(\lambda\ ([O_2] - [O_{2-offset}])) \text{ when } [O_2] > [O_{2-offset}] \quad (7)$$

Where λ is a unitless coefficient of -0.05 based the N_2O production from denitrification when $[O_2]$ are greater than 20 μM (Ji et al., 2018) and $O_{2-\text{offset}}$ is 1 μM and represents scenarios where denitrification consumes N_2O and lowers the overall N_2O production when oxygen concentrations are low enough.

$$f(O_2) = \frac{[O_2]}{[O_{2-offset}]} \text{ when } [O_2] > [O_{2-offset}] \quad (8)$$

(Capelle et al., 2018; Ji et al., 2018; Suntharalingam et al., 2012)

Note: In all scenarios, $[O_2]$ exceeded $[O_{2-\text{offset}}]$

One assumption in this calculation is that all of the oxygen consumed as part of SOD is due to organic matter decomposition and nitrogen remineralization. As

there are other biochemical processes occurring within the sediment that contribute to SOD other than nitrogen remineralization, an alternative method of calculating nitrogen remineralization was completed. This second method follows the same steps as the previous, but uses NH_4 flux rates from sediment core incubations in place of SOD to calculate N remineralization rate (Equation 9). The NH_4 flux rate may be a better proxy for nitrogen remineralization, as NH_4 flux out of the sediment is indicative of organic matter decomposition in sediment and subsequent nitrogen remineralization under both aerobic and anaerobic conditions. In this calculation it is assumed that the NH_4 flux out of the sediment is representative of organic matter decomposition to NH_4 and that nitrification rates are minimal in comparison.

$$Nitrogen\ remineralization\ rate = NH_4\ flux\ rate \times \frac{16\ mol\ N}{138\ mol\ O_2} \quad (9)$$

A third method of calculating nitrogen remineralization rate uses apparent oxygen utilization (AOU) in place of SOD:

$$Nitrogen\ remineralization\ rate = AOU \times \frac{16\ mol\ N}{138\ mol\ O_2} \quad (10)$$

AOU is substituted for SOD in this calculation because AOU is the difference between the measured concentration of oxygen in the water and the oxygen concentration at equilibrium saturation. As such, AOU represents the quantity of oxygen consumed by biological and chemical processes within the sediment and water column and is more representative of water column and sediment processes contributing to nitrogen remineralization than SOD. AOU was calculated via the following equation:

$$AOU = \frac{[O_2]_{measured\ (\mu M)}}{\frac{[O_2]_{measured\ (\%saturation)}}{100}} - [O_2]_{measured\ (\mu M)} \quad (11)$$

N_2O production rate was computed using a fourth method that defines N_2O yield as the number of moles N_2O-N per mole NO_3 produced. N_2O production rate in units of μmol N m^{-2} d^{-1} is calculated as a function of estimated nitrification rates and a previously determined N_2O-N yield coefficient of $6.70x10^{-4}$ moles N_2O-N produced per mole NO_3 produced in oxygen conditions ranging from 20-50 μM O_2 (A. Santoro, personal communication, Equation 12) and assumes that the N_2O yield and nitrification rate directly support N_2O production. Sediment nitrification rates (μmol N m^{-2} hr^{-1}) were estimated by subtracting sediment-water NO_{23}^- uptake rates from sediment N_2 production rates (Seitzinger and Nixon 1985; assuming sediment nitrification is equivalent to the N_2 fluxes not supported by direct NO_{23}^- influxes).

$$N_2O\ production\ rate = nitrification\ rate * 6.70\times10^{-4} \quad (12)$$

Results

Physical Parameters

Water temperatures in Stoney Creek, Rock Creek, and Bodkin Creek ranged from a minimum of 10.1°C in bottom waters to a maximum of 15.0°C in surface waters in April and 26.5°C in bottom waters and 32.3°C in surface waters in July. Surface and bottom water temperatures were significantly different between all creeks in April and July with the exception of April surface water temperatures (one-way ANOVA, $p < 0.05$). Salinities in each creek were within oligohaline and mesohaline regimes and significantly different in all creeks in April and July with ranges of 2.61-3.73 (one-way ANOVA, $p < 0.05$). In general, surface and bottom waters were oxygenated (>62.5 μM) at each station and creek in April and July with the exception

of bottom waters in Rock Creek during the second July sampling cruise that followed a 14-day period of no aeration. Hypoxic conditions (≤ 62.5 μM) were observed in bottom waters at Rock Creek stations 2 (Mid-Upper), 7 (Mid-Lower), and 9b (Lower) after the two-week period of inactive aeration (Figure 2.3).

Nutrient Concentrations – April

Nitrite+nitrite concentrations were elevated in all three creeks in April (Figure 2.4). NO_{23} concentrations in Rock Creek surface waters were highest in upstream stations and decreased towards the mouth of the creek. Bodkin Creek and Stoney Creek NO_{23} surface water distribution showed the inverse spatial pattern with NO_{23} concentrations increasing from upstream to downstream locations. Bottom water NO_{23} increased from upstream to downstream for all creeks in April. Peak concentrations were observed in the most upstream station in Rock Creek reaching 102.8 μM in surface waters (Figure 2.4). NO_{23} minima were observed in the bottom waters of Bodkin Creek Station 1 with a concentration of 53.3 μM. Although NO_{23} concentrations were highest in Rock Creek, surface and bottom water levels were similar for each station in all three creeks in April. In general, the distribution of NO_{23} from upstream to downstream waters was lowest in Bodkin Creek and highest in Rock Creek, indicating a potential upstream source of NO_{23} in Rock Creek (Figure 2.4). Ammonium concentrations were higher in bottom waters than surface waters for all creeks and stations with a maximum of 10.1 μM in Bodkin Creek Station 1 bottom water (Figure 2.6). Total dissolved nitrogen (TDN) distributions and patterns were similar to NO_{23} in all creeks (not plotted). Peak TDN concentrations were measured in Rock Creek Station 2 surface waters (114.2 μM) and minima in Bodkin Creek

Station 1 bottom waters (84.2 μM). TDN distribution patterns were generally similar to those of NO_{23} within the creeks with the lowest concentrations measured in Bodkin Creek and highest in Rock Creek. Particulate nitrogen (PN) was elevated in Bodkin Creek surface waters relative to Rock Creek and Stoney Creek with peak concentrations of 17.1 μM at Station 3 (Mid-Lower). Bottom water PN was highest in Rock Creek Station 7 (Mid-Lower) at 24.2 μM.

Nutrient Concentrations – July (Active Aeration)

Overall, NO_{23} concentrations were lower in surface and bottom waters in each creek during early July sampling compared to April. Peak NO_{23} levels were observed in the upstream bottom Rock Creek bottom waters with bottom water concentrations of 27.6μM, which were 1314% and 1200% higher than respective Bodkin Creek and Stoney Creek upstream bottom water concentrations (Figure 2.5). Rock Creek NO_{23} concentrations were generally higher than Bodkin Creek and Stoney Creek in surface and bottom waters. Bottom waters in Stoney Creek Stations 3 (Mid-Lower) & 4 (Lower) were the only instances that exceeded respective Rock Creek NO_{23} concentrations. Rock Creek ammonium concentrations were elevated with respect to Bodkin Creek and Stoney Creek in the two downstream stations, but lower in the two upstream stations (Figure 2.7). Peak TDN concentrations (not plotted) were measured in upstream Bodkin Creek surface waters (67.1 μM) and minima in Rock Creek Station 7 (Mid-Lower) bottom waters (15.0 μM) during aeration. PN maxima was measured in upstream Bodkin Creek surface waters (41.5 μM). Lowest PN concentrations were Bodkin Creek Station 3 (Mid-Lower) and Stoney Creek Station 3 (Mid-Lower) bottom waters (7.03 μM) in early July sampling.

Nutrient Concentrations – July (Inactive Aeration)

Rock Creek NO_{23} concentrations were similar to those of Bodkin Creek and Stoney Creek after aeration had been inactive for two weeks (Figure 2.5). There was no apparent spatial trend in Rock Creek surface and bottom waters following two weeks of inactive aeration compared to early July Bodkin Creek and Stoney Creek. Ammonium concentrations were lower in Rock Creek surface and bottom waters after inactive aeration relative to the aerated period with the exception of station 9b (Lower) bottom waters. TDN levels (not plotted) were consistently lower during inactive aeration than when aeration was ongoing. Concentrations peaked in downstream bottom waters (27.8 μM) and were lowest in Station 7 (Mid-Lower) bottom waters (15.0 μM). PN was generally higher in Rock Creek surface waters after aeration had been inactive with peak concentrations of 70.0 μM measured at Station 2 (Mid-Upper). The lowest Rock Creek PN levels were measured in Station 2 (Mid-Upper) bottom waters (12.2 μM).

Sulfide concentrations

Sulfide (not plotted) was measured in surface and bottom waters at each creek and station in April and July but only reached appreciable surface and bottom water concentrations of 5.11 μM and 0.10 μM, respectively, in Rock Creek Station 1 (Upper) after two weeks of inactive aeration (not plotted). Trace detections of 0.004 μM, 0.007 μM, and 0.007 μM were measured in surface and bottoms waters of Bodkin Creek Station 1 (Upper) and surface waters in Stoney Creek Station 1 (Upper), respectively.

Sediment-water flux

Measured sediment-water fluxes differed across all creeks and seasons (Table 2.2). NO_{23} fluxes were highest in Bodkin Creek during the spring with a peak rate of 83.7 μmol N m^{-2} hr^{-1}. Rock Creek and Stoney Creek NO_{23} fluxes are not reported due to transport and temperature issues with the sediment cores during incubation and non-interpretable data. Rock Creek sediment-water NO_{23} flux rates after inactive aeration were comparable to April with rates of 81.3 μmol N m^{-2} hr^{-1}. NO_{23} flux rates in July Bodkin Creek, Stoney Creek, and Rock Creek during active aeration were all negative with rates of -29.0, -113, and -191 μmol N m^{-2} hr^{-1}, respectively, indicating sediment NO_{23} uptake. NH_4 flux rates were negative in all creeks in April. These negative values indicate sediment uptake of NO_{23} and NH_4 but may be the result of core disturbance and temperature problems experienced during transportation. July NH_4 flux rates were all positive. April minima was measured in Rock Creek at -34.2 μmol N m^{-2} hr^{-1}. July NH_4 flux rates peaked in Rock Creek during active aeration at 386 μmol N m^{-2} hr^{-1}. The lowest NH_4 flux rate in July was measured in Bodkin Creek at 81.8 μmol N m^{-2} hr^{-1}. Sediment oxygen demand (SOD) rates in units of μmol O_2 m^{-2} hr^{-1} were quantified as the oxygen flux into the sediment during core incubations, where negative SOD values indicate sediment uptake of oxygen. SOD rates were less negative across creeks in April compared to July. SOD rates in April ranged from -310 μmol O_2 m^{-2} hr^{-1} (Stoney Creek) to -431 μmol O_2 m^{-2} hr^{-1} (Rock Creek). Only Bodkin Creek SOD rates in July were comparable to April with a measured rate of -362 μmol O_2 m^{-2} hr^{-1}. Peak July SOD rates of -2450 μmol O_2 m^{-2} hr^{-1} occurred in Rock Creek during active aeration. July SOD rates in Stoney Creek and Rock Creek

during inactive aeration were 691 and 877 μmol O_2 m^{-2} hr^{-1}, respectively.

Sediment Nitrification and Denitrification Rates

Denitrification rates were measured as N_2 flux out of the sediment during intact core incubations and ranged from -283 to 1246 μmol N m^{-2} hr^{-1} in April and 612-1572 μmol N m^{-2} hr^{-1} in July. The highest denitrification rates occurred in July Rock Creek during active aeration and dropped to 784 μmol N m^{-2} hr^{-1} after the inactive aeration period. Stoney Creek sediment yielded the lowest denitrification rates amongst the three creeks in April and July at -127 μmol N m^{-2} hr^{-1} and 612 μmol N m^{-2} hr^{-1}, respectively. The negative denitrification rate measured in Stoney Creek sediment indicates N_2 update by the sediment and is likely the result of transportation and temperature issues with the cores during incubations.

Apparent sediment nitrification rates were calculated by summing the N_2 flux out of the sediment and the NO_{23} flux into the sediment, the assumption being that NO_{23} influxes support direct denitrification and the remaining N_2 production must be supported by coupled nitrification-denitrification (Seitzinger and Nixon, 1985). Nitrification showed the same pattern as denitrification with highest rates occurring in Rock Creek sediment during the active aeration period in July at 1410 μmol N m^{-2} hr^{-1}. April rates ranged from a minimum of -127 μmol N m^{-2} hr^{-1} in Stoney Creek to a maximum of 1246 μmol N m^{-2} hr^{-1} in Rock Creek. The lowest July nitrification rates were observed in Stoney Creek at 499 μmol N m^{-2} hr^{-1}. Other nitrogen cycling pathways such as DNRA and anammox may be a possible contributing factor to N_2O production, but were not able to be quantified in this study.

Nitrous Oxide Concentrations and Fluxes

Surface and bottom water N_2O concentrations were consistently lower in July than April for each respective creek and station (Figure 2.8, Figure 2,9). Peak July N_2O concentrations were observed in Rock Creek after aeration with a maximum concentration of 27.4 ± 0.3 nM (385% above atmospheric equilibrium) in Station 1 (Upper) bottom waters after two weeks of no aeration. Peak July air-sea fluxes occurred in upstream Rock Creek waters at rates of 2.2 μmol N_2O m^{-2} d^{-1} during active and inactive aeration periods. The lowest air-sea flux rates observed in April occurred in downstream Bodkin Creek waters (Mid-Lower Station 3 and Lower Station 4) at rates of 0.7 μmol N_2O m^{-2} d^{-1}. July minima were observed in Stoney Creek with an average rate of 0.1 μmol N_2O m^{-2} d^{-1} across all four stations. Surface and bottom waters were above atmospheric N_2O equilibrium (0.330 ppb) at every station and creek in April and July. Correspondingly, each creek generated positive fluxes of N_2O to the atmosphere in April and July (Figure 2.10). The highest N_2O concentrations (44.4 ± 0.7 nM, 386% above atmospheric equilibrium) and air-sea flux (2.8 μmol N_2O m^{-2} d^{-1}) occurred in upstream (Station 1) Rock Creek surface waters in April. Nitrous oxide concentrations decreased from April to July, with a minimum of 8.0 ± 0.4 nM (111% above atmospheric equilibrium) in upstream Stoney Creek surface waters.

Nitrous Oxide Production Rates

In general, N_2O production rates for each creek were higher in July than April, reaching a maximum N_2O production rate of 22.7 μmol N m^{-2} d^{-1} in Bodkin Creek in July based on the Santoro correspondence N_2O production rate calculation (Table 2.3

and Table 2.4). This method yielded the highest April and July N_2O production rates of all four variations of the rate calculations. April and July N_2O production minimums of 0.25 μmol N m^{-2} d^{-1} and 0.12 μmol N m^{-2} d^{-1}, respectively were observed in Rock Creek and were the result of calculating N_2O production rates using AOU in the Ji et al., (2018) calculation. Bodkin Creek N_2O production rates were higher than all other creeks in July for each of the four calculations, with the exception of the SOD based rate calculation.

Discussion

Oxygen and nutrient availability are important factors in biogeochemical nitrogen cycling and its associated influence on nitrous oxide generation in estuarine systems. The data presented in this study demonstrate the significance of these controls on N_2O production in three anthropogenically-affected tributaries of the Patapsco River. All three nitrogen-rich creeks served as sources of N_2O to the atmosphere in both April and July 2019, with Rock Creek serving as the largest source. Measured N_2O concentrations in all creeks were large relative to those reported in other recent Chesapeake Bay studies. Laperriere et al., (2018) reported N_2O concentrations ranging from 9.2-20.0 nM in August and 1.7-15.3 nM in September in main stem Chesapeake Bay. Comparatively, April N_2O concentrations in this study ranged from 20.0-44.4 nM in surface waters and 20.0-38.7 nM in bottom waters. July N_2O concentrations in surface and bottom waters ranged from 8.0-26.5 nM and 8.3-27.4 nM, respectively. Engineered aeration in Rock Creek appears to impact oxygen availability and nitrogen cycling within Rock Creek in July, with N_2O production and availability enhanced under moderate oxygen depletion that

developed when the aerators were turned off.

Nutrient availability plays a large role in nitrous oxide generation, as ammonium and nitrate are necessary components of coupled nitrification-denitrification processes. Elevated NH_4^+ and NO_{23} concentrations coupled with oxic conditions in all creeks in April were associated with nitrification and subsequent N_2O production. This was especially apparent in Rock Creek during April where N_2O and NO_{23} concentrations and estimated nitrification rates exceeded those of Bodkin and Stoney Creek. Mean April N_2O concentrations in Rock Creek were 154% and 142% higher than Bodkin Creek and Stoney Creek averages, respectively. Rock Creek NO_{23} concentration means exceeded Bodkin Creek by 128% and Stoney Creek by 117%. In addition, significant positive correlations ($p<0.05$) were observed between N_2O and NO_{23} for all creeks in April and July when data were aggregated (Figure 2.11, Figure 2.12). High nitrate+nitrite concentrations in all creeks, especially during April sampling, suggest large external or internal sources and correspond to high N_2O concentrations. While the Patapsco River is a highly eutrophic estuary with high nutrient concentrations (e.g., Sellner et al., 2001; Harris et al. 2015), reported watershed nitrogen loads to Rock Creek are not exceptional on an areal basis (43 gN m^{-2} yr^{-1}, compared to nearby 50 gN m^{-2} yr^{-1} for Patapsco, 100 gN m^{-2} yr^{-1} for Back River; Boynton and Kemp, 2008; Sellner et al., 2001). In April, the spatial patterns and distributions of NO_{23} in Bodkin Creek and Stoney Creek indicated that downstream concentrations were higher than upstream, consistent with a Patapsco River nutrient source. In other Chesapeake Bay estuaries, nutrient input from downstream waters has been previously reported in cases where these higher salinity

waters are nutrient rich (e.g., Testa et al., 2008). In contrast, Rock Creek appeared to have an upstream source in April, where NO_{23} concentrations were highest upstream. Sources for these upstream inputs could include the local watershed, local submarine groundwater discharge (Moore, 1999), or internal rates of nitrification (e.g., Berounsky and Nixon 1993; Kemp et al., 1990). NO_{23} levels were lower in July than April for all creeks, suggesting lower watershed inputs or external inputs from the Patapsco (Susquehanna River flows that could influence the Patapsco were 24.8% lower in July than April; USGS Station 01578310). NO_{23} concentrations were higher in Rock Creek by a respective average of 375%, 395% and 625%, however, when aeration was active relative to Bodkin Creek, Stoney Creek, and non-aerated Rock Creek, suggesting an aeration-induced nitrification effect. For example, the highest NO_{23} concentrations measured during July were in upstream Rock Creek during active aeration (25.1 μM), as this station is the most upstream site and directly in the aeration zone (Figure 2.2). Clearly, both external inputs and internal cycling rates influence NO_{23}, with the latter leading to N_2O production.

Measurements made in this study appear to indicate high levels of nitrification, especially during July (Table 2.1 and Table 2.2). Nutrient availability plays a large role in nitrous oxide generation, as high ammonium concentrations or production in the presence of oxygen can enhance coupled nitrification-denitrification. Apparent nitrification rates in sediments increased from April to early July in all three creeks, but dropped after aeration was inactive in Rock Creek, consistent with reduced nitrification as oxygen concentrations declined with the aerators turned off (Table 2.2). The highest rates of nitrification observed were in

Rock Creek during both April and July. These rates, while similar in magnitude (1246 μmol N m^{-2} d^{-1} in April and 1410 μmol N m^{-2} d^{-1} in July during aeration), are more than double the maximum rates calculated in Narragansett Bay mesocosm experiments from Seitzinger and Nixon (1985). Sediment nitrification rates calculated in that study ranged from 309-602 μmol N m^{-2} d^{-1} in Narragansett Bay mesocosm experiments with peak rates occurring in sediments exposed to DIN loading rates of 3,900 μmol N m^{-2} hr^{-1}, 32 times higher than the control group. Additional sediment nitrification rate studies (e.g., Billen 1978; Hansen et al., 1981; Henriksen 1980; Henriksen et al., 1981) report much lower rates in North Sea and Danish fjord sediments (30-120 μmol N m^{-2} d-1). Rates from Tama Estuary, Odawa Bay, and Tokyo Bay ranged from 10-40 μmol N m^{-2} d^{-1}, much lower than those in Rock Creek, Stoney Creek, and Bodkin Creek (Nishio et al., 1982). A more local study by Jenkins and Kemp, (1984) estimated nitrification-denitrification rates of 156 and 241 μmol N m^{-2} d^{-1} in Patuxent River sediments in April 1981. The similarity of nitrification rates in Rock Creek during active aeration to those reported in April suggests that oxygen availability supports elevated nitrification, with the exception of Stoney Creek April rates. The negative rates in Stoney Creek may not be representative of the actual nitrification rates in the sediment core, but are likely erroneous due to issues in maintaining *in situ* core temperatures during the incubation. The increase in nitrification rates in all creeks in warmer months may also be attributed to increased microbial activity in warmer conditions, facilitating the oxidation of NH_4^+ to NO_3^- (Strauss et al., 2004). NO_{23} levels were lower in bottom waters despite the increase in nitrification rates, likely due to lower oxygen availability associated with warmer

conditions and microbial respiration. This is supported by the positive correlations observed between dissolved oxygen and NO_{23} across all creeks, especially in bottom waters (Figure 2.11, Figure 2.12).

Denitrification rates followed the same pattern as nitrification from April to July and may also explain the decrease in NO_{23} across seasons. The increases in nitrification and denitrification are consistent with the close coupling of these processes (Jenkins and Kemp, 1984; Nielsen et al., 2004). As surface and bottom waters were oxic in April and temperature was lower, denitrification rates were not as high possibly due to inhibition by oxygen, presuming high oxygen penetration rates into sediments (Oh and Silverstein, 1999; Von Schulthess et al., 1994), allowing for NO_{23} accumulation. A review by Seitzinger (1988) states that oxygen levels of 6.5 μM or less are required in order for denitrification to occur in sediments or the water column. While bottom water oxygen levels in July never reached that threshold, it is likely that the drop in oxygen in concert with lower sediment oxygen penetration and higher temperatures may have facilitated elevated denitrification rates in the sediments relative to April, leading to consumption of NO_{23}. Hypoxia was observed only in Rock Creek Stations 2 (Mid-Upper), 7 (Mid-Lower), and 9b (Lower) after inactive aeration, but no data regarding sediment nitrification and denitrification rates is available at the time of writing. Sulfide did not appear to impede nitrification given the elevated rates in April and July and minimal detections of sulfide outside of one sample at Rock Creek Station 1 (Upper). The nominal measured sulfide concentrations are consistent with water column oxygen never reaching anoxic conditions that would allow sulfide to accumulate (Joye and Hollibaugh, 1995).

Oxygen availability plays a large role in nitrification and the subsequent generation of N_2O, and high N_2O concentrations are observed under both high and low oxygen concentration, suggesting different N_2O production pathways in April and July. While April N_2O concentrations were larger than July, the highest N_2O concentrations measured in July occurred in bottom waters of Rock Creek under conditions of moderate oxygen depletion (Figure 2.9, Figure 2.13). This suggests a seasonal peak in nitrification in spring (Kemp et al., 1990) that corresponds with N_2O generation via nitrification combined with minimal consumption by denitrification due to oxygen inhibition and elevated NO_{23} concentrations in spring compared to summer.

Nitrification and denitrification rates in Rock Creek were lower during inactive aeration compared to the actively aerated period. This is likely the result of lower NO_3^- availability due to moderate oxygen depletion, resulting in the decreased coupled nitrification-denitrification rates. Strong positive correlations were found between oxygen and NO_{23} in July bottom waters, supporting this conclusion (Figure 2.11). Lower denitrification rates during inactive aeration also support the observation of the highest N_2O concentrations and fluxes occurring during this period. A decrease in denitrification limits N_2O consumption during reduction of NO_3^- to N_2 and thus increased N_2O concentrations compared to early July (Schipper et al., 2005; Quick et al., 2019). A 2018 study by Ji et al. reported that the highest rates of N_2O production in the Eastern Tropical Pacific occurred at the oxic-anoxic interface. Similarly, Yoshinari (1976) measured maximum N_2O concentrations at the oxygen minimum layer in the Gulf Stream between Halifax and Bermuda as well as in the Sargasso Sea.

Although anoxia was never reached in any creeks, sediments likely reached anoxic levels, typical of marine sediments (Cai & Sayles, 1996). Another potential mechanism for the elevated N_2O after inactive aeration may be N_2O generation, but not consumption, from incomplete denitrification. Incomplete denitrification occurs when the reduction of NO_3^- to N_2 is halted before the N_2O intermediate species is reduced to N_2 in the final step of the process. Oxygen inhibits the enzyme that catalyzes this final step, and if enough oxygen is present to hinder that reduction, N_2O is generated rather than being reduced to N_2 (Barnes and Owens, 1999; Hanaki and Matsuo, 1992; Jensen et al., 1984; Ligi et al., 2013; Otte et al., 1996; Palta et al., 2013; Tiedje, 1988). Even though denitrification rates were lower after inactive aeration and oxygen levels were moderately depleted, the presence of oxygen may have been enough to facilitate incomplete denitrification and thus allow the process to act as a net N_2O production pathway, as has been demonstrated in laboratory and field studies (Bonin et al, 2002; Bourbonnais et al., 2017; Hanaki and Matsuo, 1992; Quick et al., 2019). Additional studies have reported the highest N_2O production occurring in low oxygen and elevated NO_x conditions

N_2O production rates calculated as a function of N_2O yields from nitrification (Table 2.1 and Table 2.2) were lower in April than July in all creeks, with the exception of Rock Creek. The peak N_2O production rate for Rock creek of 20.0 µmol N m^{-2} d^{-1} in April was calculated using a simple function of derived nitrification rates and oxygen concentration (Alyson Santoro, personal communication). Using the same approach, N_2O production rates during. July in Rock Creek were lower, including estimated rates of 19.1 µmol N m^{-2} d^{-1} with aeration and 13.7 µmol N m^{-2}

d^{-1} without aeration. Given the negative nitrification rates and NH_4 fluxes reported from spring sediment-core incubations, this version of the calculation may not be representative of the actual N_2O production rates. For this reason, N_2O production rates calculated with AOU (Ji et al., 2018) are discussed, as AOU is more representative of community-wide oxygen consumption in both the water column and sediments (Table 2.2). Spring N_2O production rates were similar in magnitude in all creeks (0.25-0.31 μmol N m^{-2} d^{-1}) and increased in summer aside from aerated Rock Creek, which decreased from 0.25 μmol N m^{-2} d^{-1} to 0.12 μmol N m^{-2} d^{-1}. The generally higher summer N_2O production rates might suggest lower N_2O levels in the spring compared to summer, but highest N_2O concentrations were measured in April. A 1999 study by de Wilde and de Bie reported increased N_2O yield from incomplete nitrification at oxygen concentrations of ~70 μM. These observations of increased N_2O yield in oxygen-depleted conditions are consistent with laboratory (Goreau et al., 1980), Potomac River (McElroy et al., 1978), and Hudson River estuarine studies (Deck, 1982). A similar increase in N_2O production rates (and yield) in moderate oxygen depletion conditions is seen in July, especially in Bodkin Creek (4.60 μmol N m^{-2} d^{-1}) and in Rock Creek without aeration (1.65 μmol N m^{-2} d^{-1}). The higher N_2O production rates in July may reflect partial nitrification and subsequent increases in N_2O yields, as bottom water oxygen concentrations were 66 μM in Bodkin Creek and 85 μM in Rock Creek, and denitrification rates were highest in July in aerated Rock Creek at 1572 μmol N m^{-2} hr^{-1} (Blackburne et al., 2007; Jianlong and Ning, 2004). The low N_2O production rates in Rock Creek with aeration (0.12 μmol N m^{-2} d^{-1}) may be the result of low AOU (51 μM), as oxygen was measured at 192 μM. The N_2O

production rates calculated from N_2O yields in both April and July (Ji et al., 2018, AOU method) are comparable to those measured in other studies. Santoro et al., (2010) reported N_2O production rates of 0.88-2.29 μmol N m^{-2} d^{-1} in the Central California current and N_2O production rates calculated in this study ranged from 0.12-4.60 μmol N m^{-2} d^{-1}, respectively, with the Ji et al., (2018) AOU method (Table 2.2).

Nitrification rates in this study are computed as a function of measured denitrification rates and the concentration of NO_{23} required for denitrification (Seitzinger and Nixon, 1985). As such, the high denitrification rates measured in this study help drive the high nitrification rates computed. Excluding denitrification rates from April Stoney Creek (-38.9 μmol N m^{-2} hr^{-1}) due to temperature and transport issues with the cores, measured denitrification rates in all scenarios are extremely high relative to studies in areas of high organic matter and NO_{23} availability (i.e. estuarine marshes, WWTPs, estuarine turbidity maximum zones). A study of sediment-water nitrogen exchange in Potomac River (Cornwell et al., 2015) measured average spring and summer denitrification rates of 153 ± 97 μmol N m^{-2} hr^{-1} and 54 ± 47 μmol N m^{-2} hr^{-1}, respectively. Spring denitrification rates ranged from 0-364.2 μmol N m^{-2} hr^{-1} and 0-174.4 μmol N m^{-2} hr^{-1} in summer. Bodkin Creek and Rock Creek April denitrification rates were measured at 283 ± 86 μmol N m^{-2} hr^{-1} and 1246 ± 247 μmol N m^{-2} hr^{-1}, respectively, ~1.9 and 8.1 times higher than Potomac River spring denitrification rates, although spring Bodkin Creek denitrification rates were comparable and within the ranges measured by Cornwell et al. (2015). July denitrification rates were higher than April for each respective creek, with the

exception of Rock Creek without aeration. The lowest July denitrification rates (Stoney Creek, 612 ± 0.61 μmol N m^{-2} hr^{-1}) are 11 times higher than Potomac River summer denitrification rates. Denitrification rates in oligohaline marshes were reported at ~60 μmol N m^{-2} hr^{-1} (Merrill and Cornwell, 2002) and 1.43 μmol N m^{-2} hr^{-1} in an area of the Seine River estuary affected by WWTP discharge (Sebilo et al., 2006). The substantially high denitrification rates measured in April and July in all creeks likely contribute to the elevated N_2O levels in both seasons, or are co-occurring with high nitrification rates that generate N_2O and support denitrification. NO_{23} availability through tidal or upstream input, or generation by NH_4^+ oxidation to NO_3^- is likely fueling these high denitrification rates, especially in warmer months when nitrification rates are increased. Even in July when denitrification rates were higher than April, there is potential for incomplete denitrification to contribute to net N_2O production.

A recent study by Laperriere et al., (2018) reported surface water air-sea N_2O flux estimates of 4 μmol N_2O m^{-2} d^{-1} in main stem Chesapeake Bay from a three-layer box model and maximum observed N_2O concentrations of 20.9 nM in August 2013. Surface water N_2O concentrations from this study were almost uniformly higher in April than these reported measurements, but air-sea fluxes were lower (2.8 μmol N_2O m^{-2} d^{-1} maximum in upstream Rock Creek). July fluxes were similar in magnitude to April with maximum fluxes of 2.2 μmol N_2O m^{-2} d^{-1} in Rock Creek Station 1 (Upper) surface waters during active and inactive aeration, but overall average flux across seasons was lower (2.1 μmol N_2O m^{-2} d^{-1} average in April and 1.2 μmol N_2O m^{-2} d^{-1} average in July for Rock Creek). This seasonal decrease in air-sea flux is likely a

product of the overall lower N_2O concentrations observed in July compared to April. Air-sea fluxes in Rock Creek, Stoney Creek, and Bodkin Creek in April and July were consistently lower than those reported by Laperriere et al., (2018). This variability may be partially attributed to the limited exposure of the Patapsco River tributaries to winds. Rock Creek, Bodkin Creek, and Stoney Creek are more protected than main stem Chesapeake Bay and likely experience lower wind speeds than open waters, which would contribute to lower average N_2O fluxes. Laperriere et al., (2018) reported 20-knot (10.2 m s^{-1}) wind events for both of the sampling trips. The highest wind speeds reported in this study were 2.5 knots (1.3 m s^{-1}). Bange et al., (1996) estimated air-sea N_2O fluxes from surface waters in the Aegean Sea in July 1993 and reported an average air-sea flux rate of 1.04 ± 1.12 μmol N_2O m^{-2} d^{-1}, attributed to a mean surface water N_2O 103% higher than atmospheric equilibrium. Comparatively Rock Creek surface waters were 317 and 244% N_2O above atmospheric equilibrium in April and July, respectively. A study of numerous United Kingdom estuaries (Barnes and Upstill-Goddard, 2011) reports measurements of N_2O ranges of 140-2000% above atmospheric equilibrium in the anthropogenically affected Tees estuary. Average surface water N_2O levels in April Rock Creek, Bodkin Creek, and Stoney Creek were 317, 217, and 217% above atmospheric equilibrium, respectively. July averages were 244, 172, and 114% for Rock Creek, Bodkin Creek and Stoney Creek. Zhan et al., (2017) report maximum air-sea flux rates of 21.0 ± 3.9 μmol N_2O m^{-2} d^{-1} in tropical and sub-tropical regions, and 9.8 ± 0.5 μmol N_2O m^{-2} d^{-1} maximums in the Southern Ocean. Although these air-sea fluxes are higher than those measured in this study, this is likely due to higher exposure to elevated wind speeds in an ocean

system compared to sub-tidal estuarine tributaries. A review by Murray et al., (2015) reported a median N_2O flux of 18.2 μmol N_2O m^{-2} d^{-1} based on a collection of 23 reports measuring N_2O air-water flux in estuarine open water systems. In general, the magnitude of air-sea fluxes and surface water N_2O elevation relative to atmospheric equilibrium observed in this study are comparable to similarly anthropogenically-impacted systems, in particular, those in Chesapeake Bay.

Despite the air-water fluxes of N_2O from Rock Creek waters to the atmosphere, the magnitude of these fluxes was extremely small within the context of nitrogen budgets in Rock Creek. Although nitrogen budgets are not available for Bodkin Creek or Stoney Creek, a recent report (Harris and Testa, 2019) listed Rock Creek N inputs of 157,189 kg N yr^{-1} and loses of 150,448 kg N yr^{-1} during active aeration and inputs of 157,189 kg N yr^{-1} and loses of 120,983 kg N yr^{-1} without aeration (Boynton et al., 2008; Boynton and Kemp, 2008; CH2M, 2011; Testa et al., 2013). The yearly basin-wide N_2O flux for Rock Creek contributes only 0.036% to the total N inputs in aerated and non-aerated scenarios. Similarly, yearly basin-wide flux is estimated to contribute 0.038% and 0.047% to the total N losses in aerated and non-aerated scenarios, respectively. These values were calculated by applying the average yearly N_2O air-water flux (μmol N_2O m^{-2} d^{-1}) from Rock Creek based on the data collected in this study to the basin area of the creek. Units were then converted from μmol N_2O d^{-1} to kg N_2O-N yr^{-1}. While Rock Creek, Bodkin Creek, and Stoney Creek are demonstrated to be sources of N_2O to the atmosphere, the overall contribution to the yearly Rock Creek N budget are minimal. N_2O fluxes are trivial within the context of nitrogen budgets, but elevated concentrations with respect to

equilibrium and calculated fluxes are similar to other estuarine environments (Bange et al., 1996; Barnes and Upstill-Goddard, 2011; Laperriere et al., 2018). The same calculation was carried out for Chesapeake Bay. For this calculation it was assumed that the average yearly N_2O flux rate for Rock Creek estimated in this study is representative of Chesapeake Ba-wide fluxes. This may be an underestimation of actual Chesapeake Bay N_2O fluxes as Bay-wide open water wind speeds are likely higher than those in the protected Rock Creek basin. Based on this assumption, Chesapeake Bay emits ~181,000 kg N_2O-N yr^{-1}, 0.16% of the yearly N watershed load, and a mere 0.06% of the 0.31 Tg N_2O-N emitted by estuarine ecosystems globally (USEPA, 2010). Although the contribution of Chesapeake Bay to the global N_2O emissions and watershed N load is small, the 181,000 kg N_2O-N yr^{-1} emitted is the CO_2 equivalent of burning 9.5 million gallons of gasoline. It is important to continue to quantify N_2O in regions like Chesapeake Bay in order to better constrain the N_2O emissions, especially given the potential for increased anthropogenic nitrogen loading to these systems.

Summary

The data collected in this study demonstrate the importance of nutrient and oxygen availability on nitrous oxide production in estuarine systems. Oxygen availability appears to directly influence nitrification rates and subsequent N_2O production. This is especially apparent in Rock Creek during July sampling, as N_2O levels were elevated relative to Bodkin Creek and Stoney Creek (Figure 2.9, Figure 2.13). Nitrous oxide is highest in scenarios of high nutrient and oxygen availability likely due to elevated production via nitrification. Elevated NO_{23} measured in April

supports the hypothesis that build up of NO_{23} is likely from nitrification production and the inhibition of denitrification and subsequent reduction of NO_3^- to N_2 gas due to the presence of oxygen. In moderate oxygen depletion, (i.e. Rock Creek without aeration), nitrous oxide remains elevated, but less so than in April. One possible explanation is that N_2O is being produced by nitrification and incomplete denitrification, as oxygen levels may have been high enough to inhibit the consumption of N_2O during denitrification. Denitrification rates were substantially high in April and July and may be attributed to high NO_{23} loads in spring and NO_3^- generation in July from elevated nitrification. Bodkin and Stoney exhibit similar patterns of N_2O production when compared to Rock Creek, but on a lesser scale. Although the influence of the Patapsco River on NO_3^- levels was clear in Bodkin and Stoney Creeks in April but not in Rock Creek, nitrogen budgets suggest that the Patapsco is a large source of nitrogen to Rock creek as well, supporting high rates of denitrification. All creeks were sources of N_2O to the atmosphere in April and July, with highest fluxes associated with the highest N_2O concentrations, but comparable to those reported in similar estuarine and coastal studies. These findings help broaden our understanding of N_2O cycling, availability, and distributions within estuarine ecosystems in scenarios of varying nutrient and oxygen availability.

Future Directions

The nitrous oxide data collected in this study are some of the first of its kind for Rock Creek, Bodkin Creek, and Stoney Creek, but continued research is necessary to further elucidate mechanisms behind N_2O controls and distributions in anthropogenically-affected waters. Additional sampling in autumn may provide

useful insight into seasonal variations in N_2O production, and sediment core collection from additional stations, though cumbersome, will allow for better understanding of nitrification-denitrification rates within the tidal axes of the creeks. The incorporation of sediment flux modeling (Di Toro, 2001; Testa et al., 2013) can help simulate N_2O yields and potential N_2O fluxes from estuarine systems and would be a valuable supplement to understanding N_2O distribution under varying oxygen and nutrient loading scenarios. Experiments to directly quantify nitrification rates, DNRA, and anammox within the water column and sediment, coupled with N_2O measurements in sediment may allow for more representative N_2O production rate estimations and understanding of the processes that are contributing to N_2O generation. Additional linear modeling and means comparisons of various parameters will be completed to help further the understanding of controls on nitrous oxide in coastal and estuarine systems.

Tables

Table 2.1 Rock Creek, Stoney Creek, and Bodkin Creek characteristics. Volume and surface area from Cronin & Pritchard, (1975). Station depth, salinity, and temperature ranges are relative to the data collected in this study.

Creek	Volume (10^6 m^3)	Surface area (10^6 m^2)	Station depth range (m)	Salinity range	Temperature range (˚C)
Rock Creek	9.60	3.61	2.5 – 4.0	3.1 – 4.1	10.1 – 32.3
Stoney Creek	8.99	2.74	2.0 – 3.0	3.1 – 4.0	10.7 – 29.7
Bodkin Creek	5.06	2.31	2.5 – 4.5	2.4 – 3.5	10.8 – 28.7

Table 2.2 Sediment-flux rates (means ± standard deviation) of each station and date for N_2, NH_4^+, NO_{23}, SOD, and AOU. Values marked with * denote single cores with no calculated standard deviation. No data (ND) is available for three data points due to correlation coefficients <0.85 (see *Sample Collection)*.

Station	Date	N_2 Denitrification (µmol N m^{-2} hr^{-1})	Apparent Nitrification rate (µmol N m^{-2} hr^{-1})	NH_4 (µmol N m^{-2} hr^{-1})	NO_{23} (µmol N m^{-2} hr^{-1})	SOD (µmol O_2 m^{-2} hr^{-1})	AOU (µM)
Bodkin Creek 1	4/8/19	283 ± 86	367	ND	83.7*	431*	126
Rock Creek 1	4/8/19	1246 ± 247	1246	-34.2 ± 15	ND	409 ± 197	109
Stoney Creek 1	4/8/19	-127 ± 126	-127	-27.0 ± 38	ND	310*	134
Rock Creek 1 (aerated)	7/9/19	1572 ± 159	1410	386 ± 70	-191 ± 41	2450 ± 170	51.4
Bodkin Creek 1	7/10/19	1218 ± 415	1189	81.8 ± 31	-29.0*	362*	177
Stoney Creek 1	7/10/19	612 ± 0.6	499	118 ± 24	-113*	691 ± 277	153
Rock Creek 1 (non-aerated)	7/22/19	784 ± 204	850	159 ± 20	81.3 ± 21	877 ± 325	148

Table 2.3 Comparison of apparent nitrification rates, N_2O production rates generated by the four varying calculations, and N_2O concentrations for April 2019 sediment-core stations. ND (no data) is available for N_2O production rates calculated using NH_4 flux and Stoney Creek using the Santoro correspondence calculation method due to negative NH_4 fluxes and nitrification rates.

Station	**Apparent Nitrification rate (µmol N m^{-2} hr^{-1})**	**N_2O production rate using SOD (µmol N m^{-2} d^{-1}) (Ji et al., 2018)**	**N_2O production rate using NH_4 flux (µmol N m^{-2} d^{-1}) (Ji et al., 2018**	**N_2O production rate using AOU (µmol N m^{-2} d^{-1}) (Ji et al., 2018**	**N_2O production rate (µmol N m^{-2} d^{-1}) (Santoro correspondence)**	**Bottom water [N_2O] (nM)**
Bodkin Creek 1	367	0.99	ND	0.29	5.89	25.3 ± 0.5
Stoney Creek 1	-127	0.71	ND	0.31	ND	26.9 ± 0.3
Rock Creek 1	1246	0.92	ND	0.25	20.0	38.8 ± 0.8

Table 2.4 Comparison of apparent nitrification rates, N_2O production rates generated by the four varying calculations, and N_2O concentrations for July 2019 sediment-core stations.

Station	Apparent Nitrification rate (µmol N m^{-2} hr^{-1})	N_2O production rate using SOD (µmol N m^{-2} d^{-1}) (Ji et al., 2018)	N_2O production rate using NH_4 flux (µmol N m^{-2} d^{-1}) (Ji et al., 2018	N_2O production rate using AOU (µmol N m^{-2} d^{-1}) (Ji et al., 2018	N_2O production rate (µmol N m^{-2} d^{-1}) (Santoro correspondence)	Bottom water [N_2O] (nM)
Bodkin Creek 1	1189	9.39	2.12	4.60	22.7	9.8 ± 0.4
Stoney Creek 1	499	3.27	0.56	0.72	8.03	8.3 ± 0.1
Rock Creek 1 (aerated)	1410	5.63	0.89	0.12	19.1	26.5 ± 0.2
Rock Creek 1 (non-aerated)	850	9.76	1.77	1.65	13.7	27.4 ± 0.6

Figures

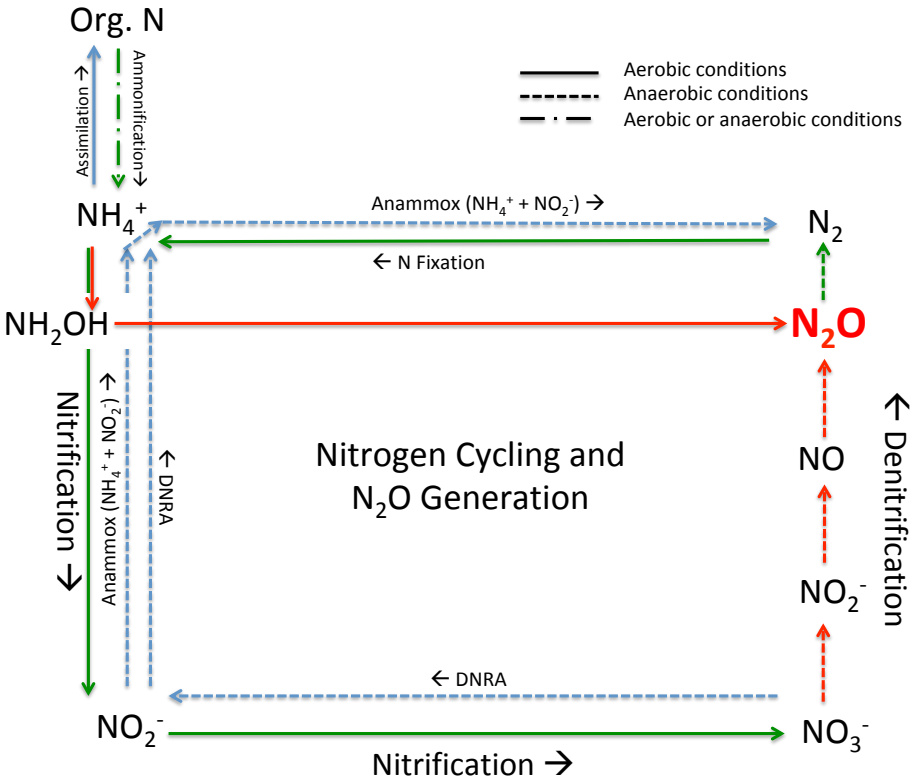

Figure 2.1 Conceptual diagram demonstrating N cycling and N_2O production pathways in estuarine systems.

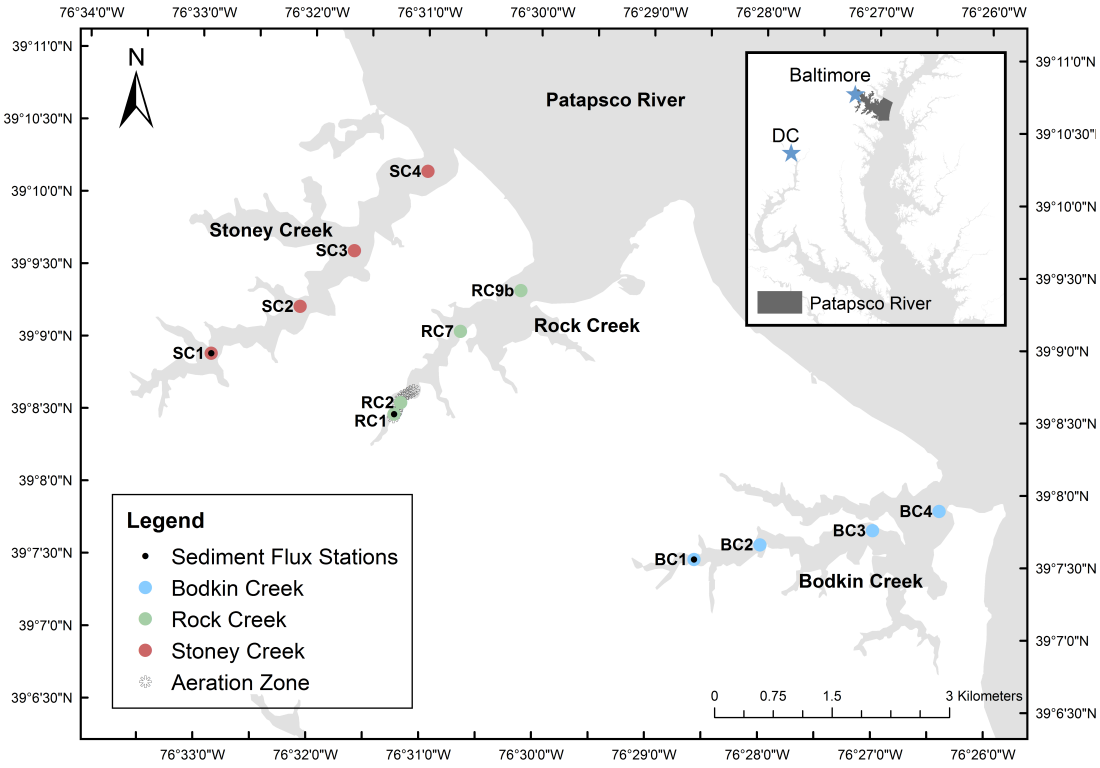

Figure 2.2 Map of Stoney Creek, Rock Creek, and Bodkin Creek estuaries and location within the larger Chesapeake Bay. Colored circles represent locations of sample sites within each creek.

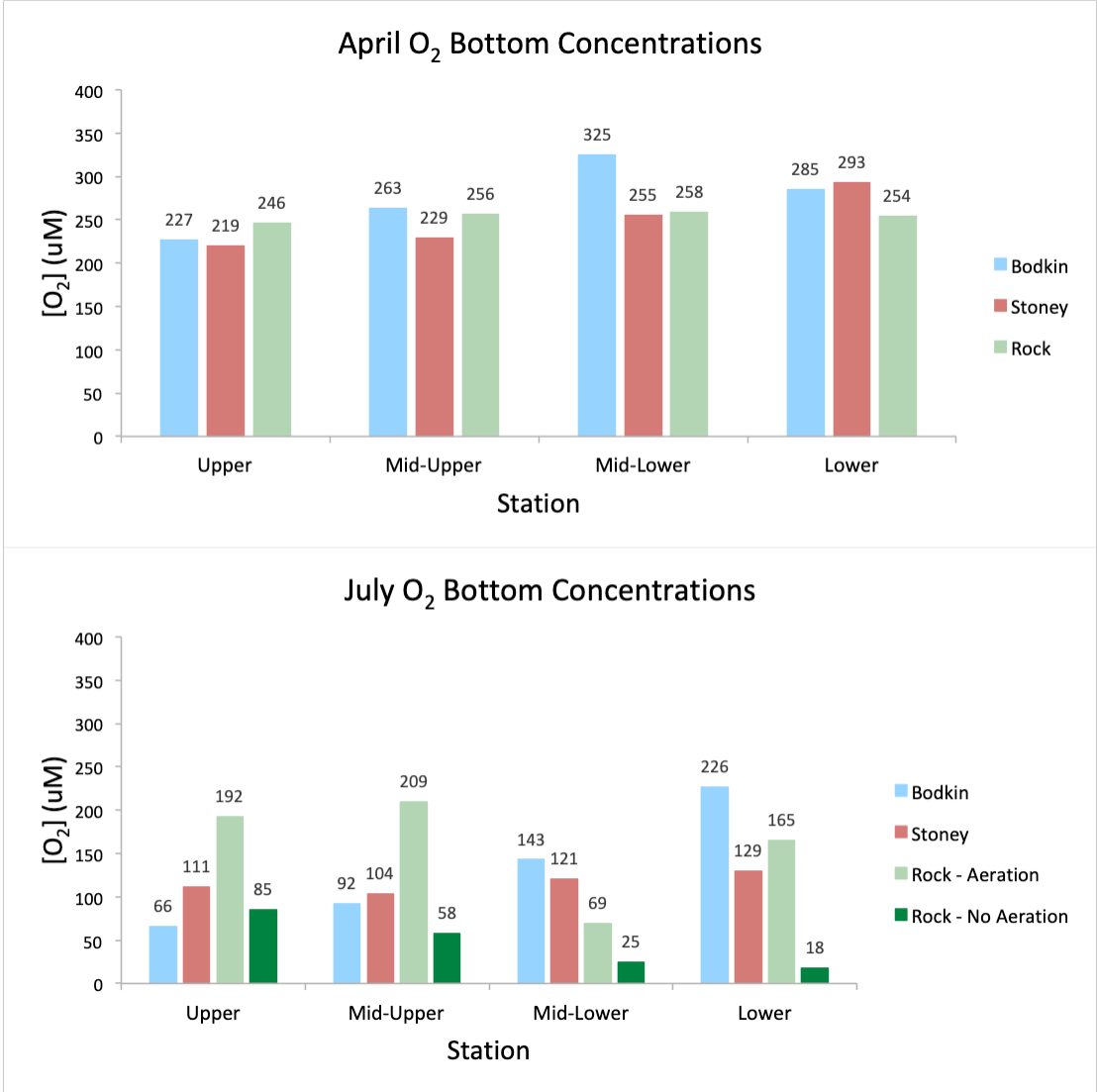

Figure 2.3 April and July bottom water O_2 concentrations (μM) for Bodkin Creek, Stoney Creek, and Rock Creek. Rock Creek sampled twice in July – once during active aeration and again after two weeks of inactive aeration. Note hypoxic conditions reached only in Rock Creek Stations 2 (Mid-Upper), 7 (Mid-Lower), and 9b (Lower) after inactive aeration period.

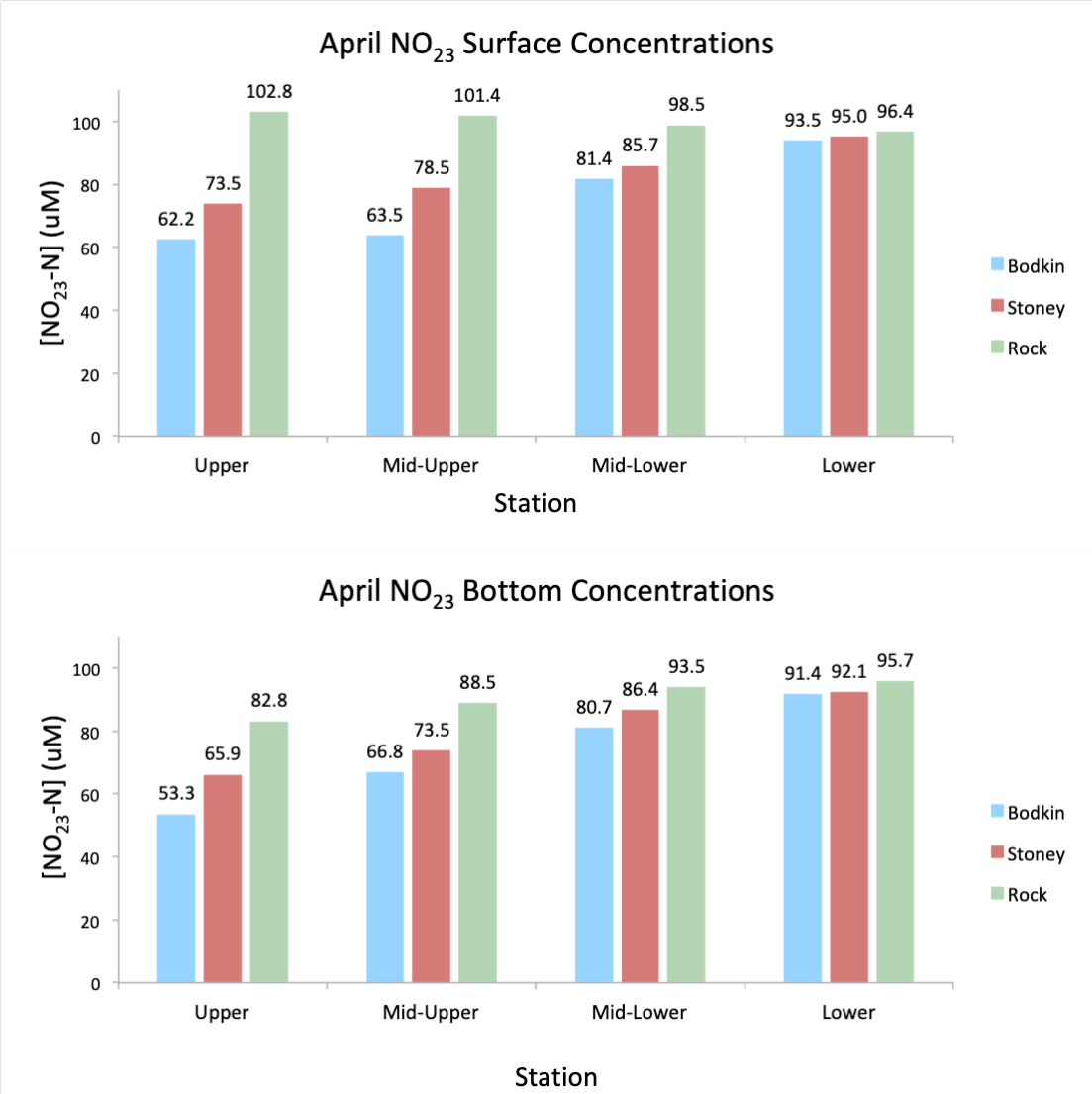

Figure 2.4 April surface and bottom water NO_{23}-N concentrations (µM) for Bodkin Creek, Stoney Creek, and Rock Creek. Rock Creek had highest levels of NO_{23} in upstream waters indicating am upstream nutrient source. Bodkin Creek and Stoney Creek appear to have a Patapsco River nutrient influence.

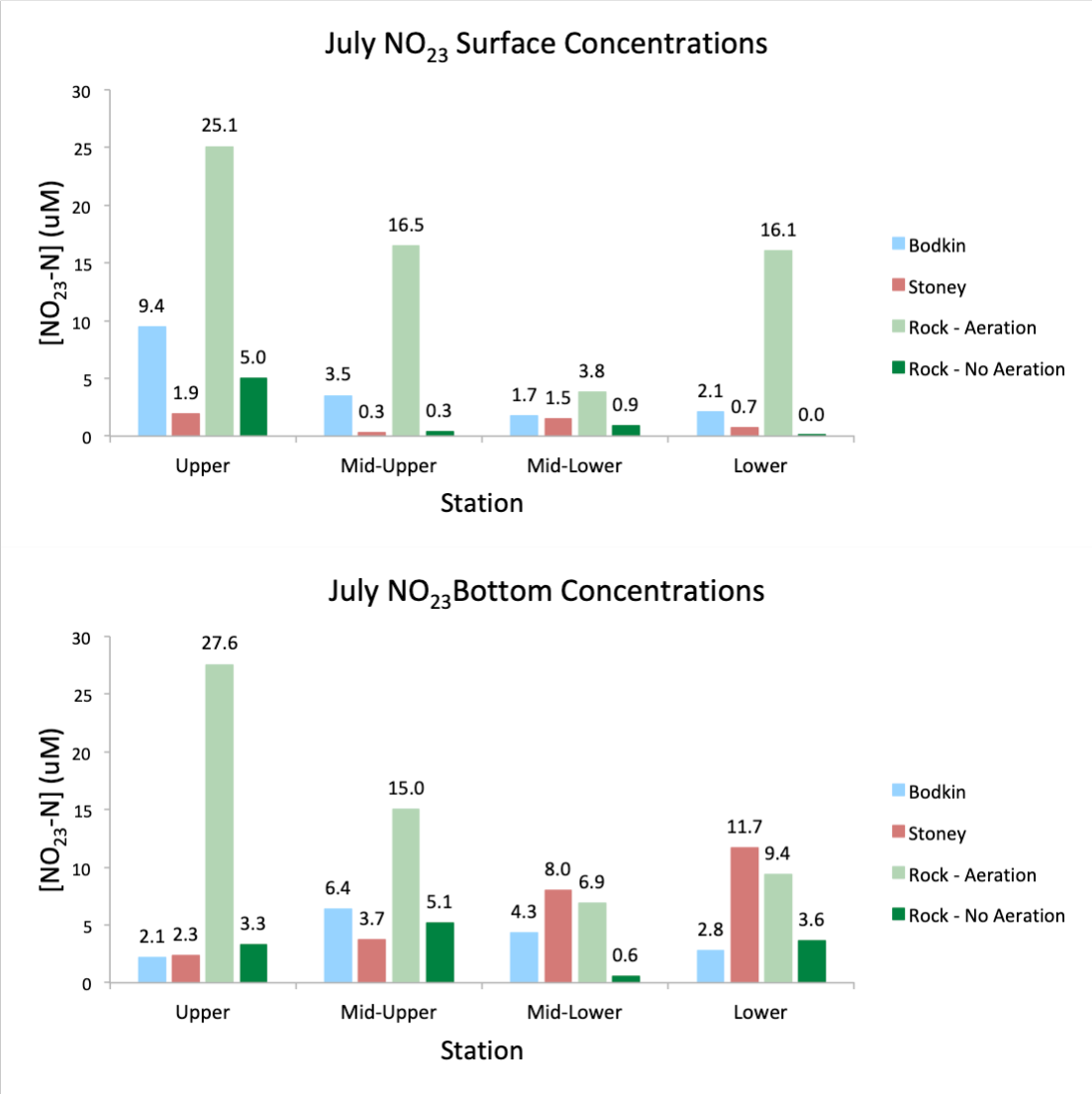

Figure 2.5 July surface and bottom water NO_{23}-N concentrations (µM) for Bodkin Creek, Stoney Creek, and Rock Creek. Note elevated NO_{23} concentrations in upstream Rock Creek (Station 1) during active aeration. Rock Creek Stations 1 (Upper) and 2 (Mid-Upper) are located within the aeration zone.

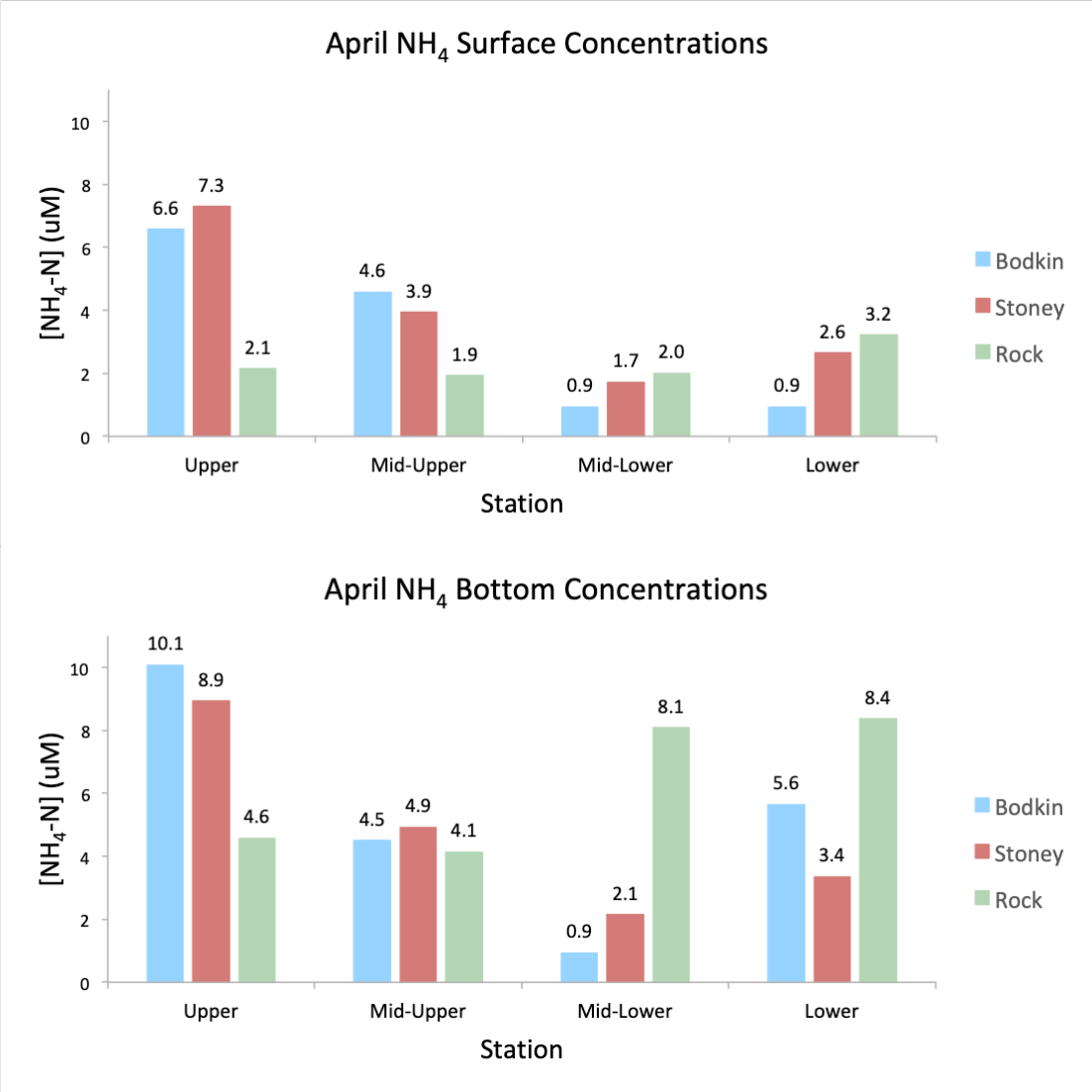

Figure 2.6 April surface and bottom water NH_4-N concentrations (µM) for Bodkin Creek, Stoney Creek, and Rock Creek. Concentrations are generally elevated in bottom waters relative to surface waters in all creeks.

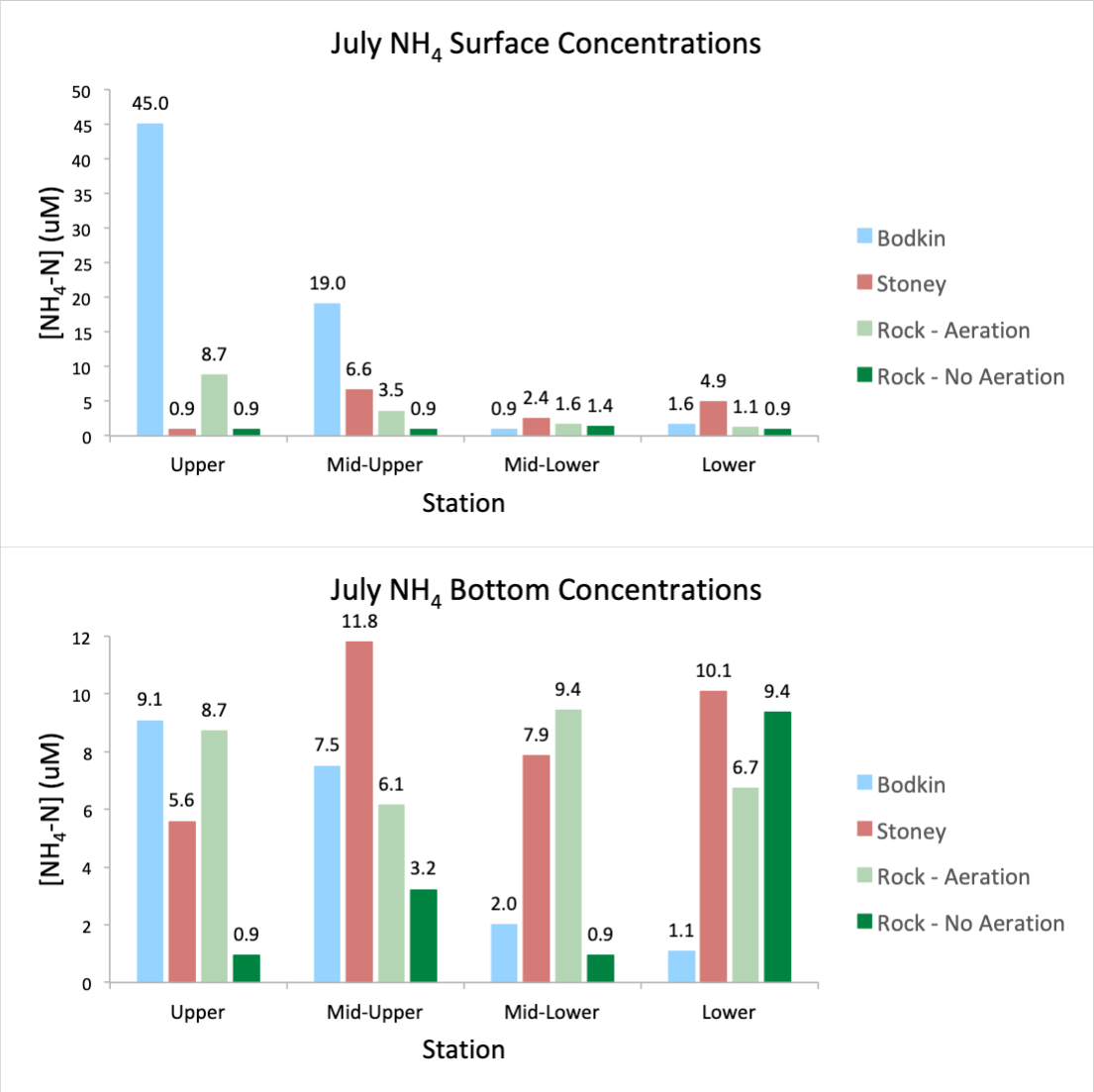

Figure 2.7 July surface and bottom water NH_4-N concentrations (µM) for Bodkin Creek, Stoney Creek, and Rock Creek.

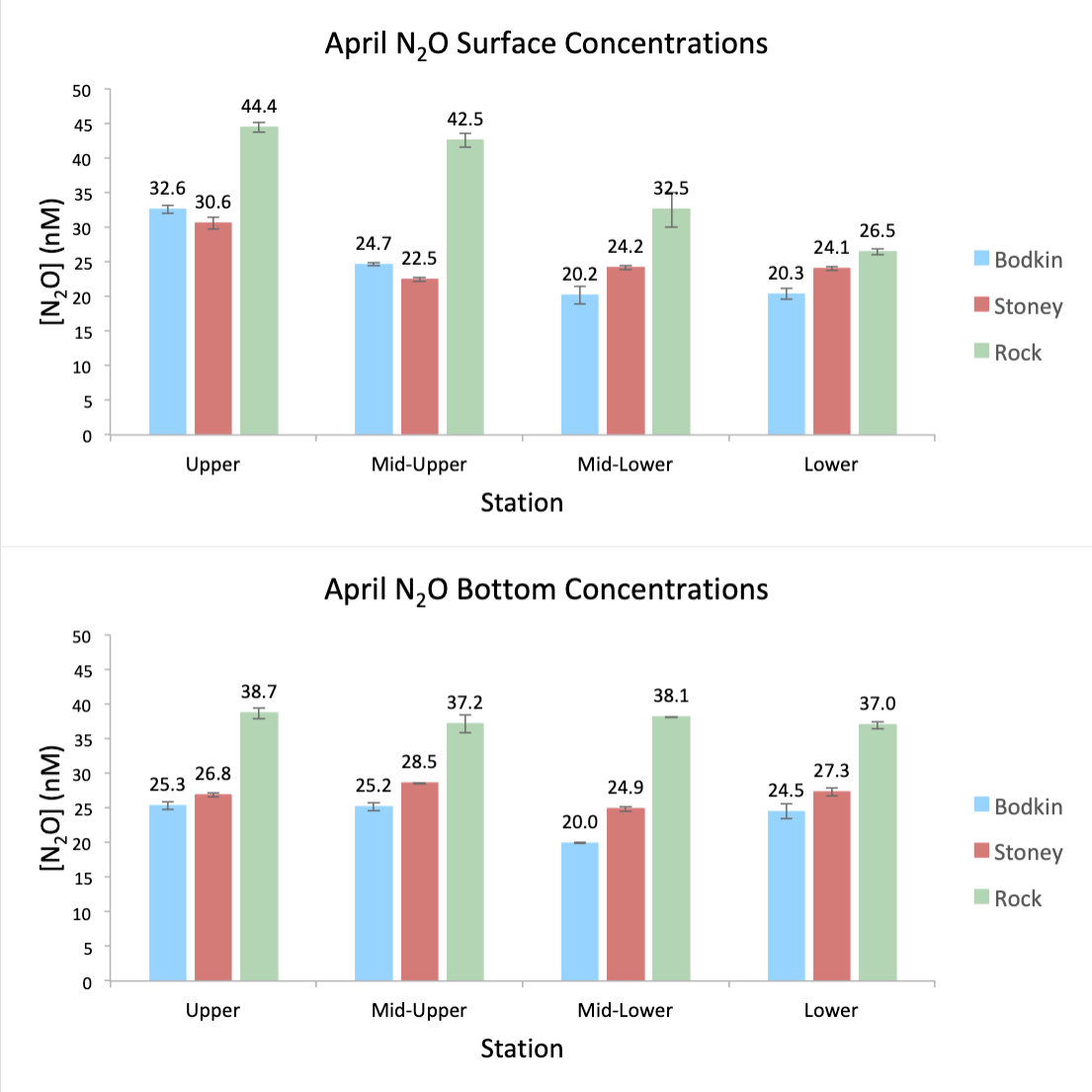

Figure 2.8 April surface and bottom water N_2O concentrations (nM) for Bodkin Creek, Stoney Creek, and Rock Creek. N_2O concentrations are highest in Rock Creek and decrease from upstream to downstream stations. All waters were above atmospheric N_2O equilibrium.

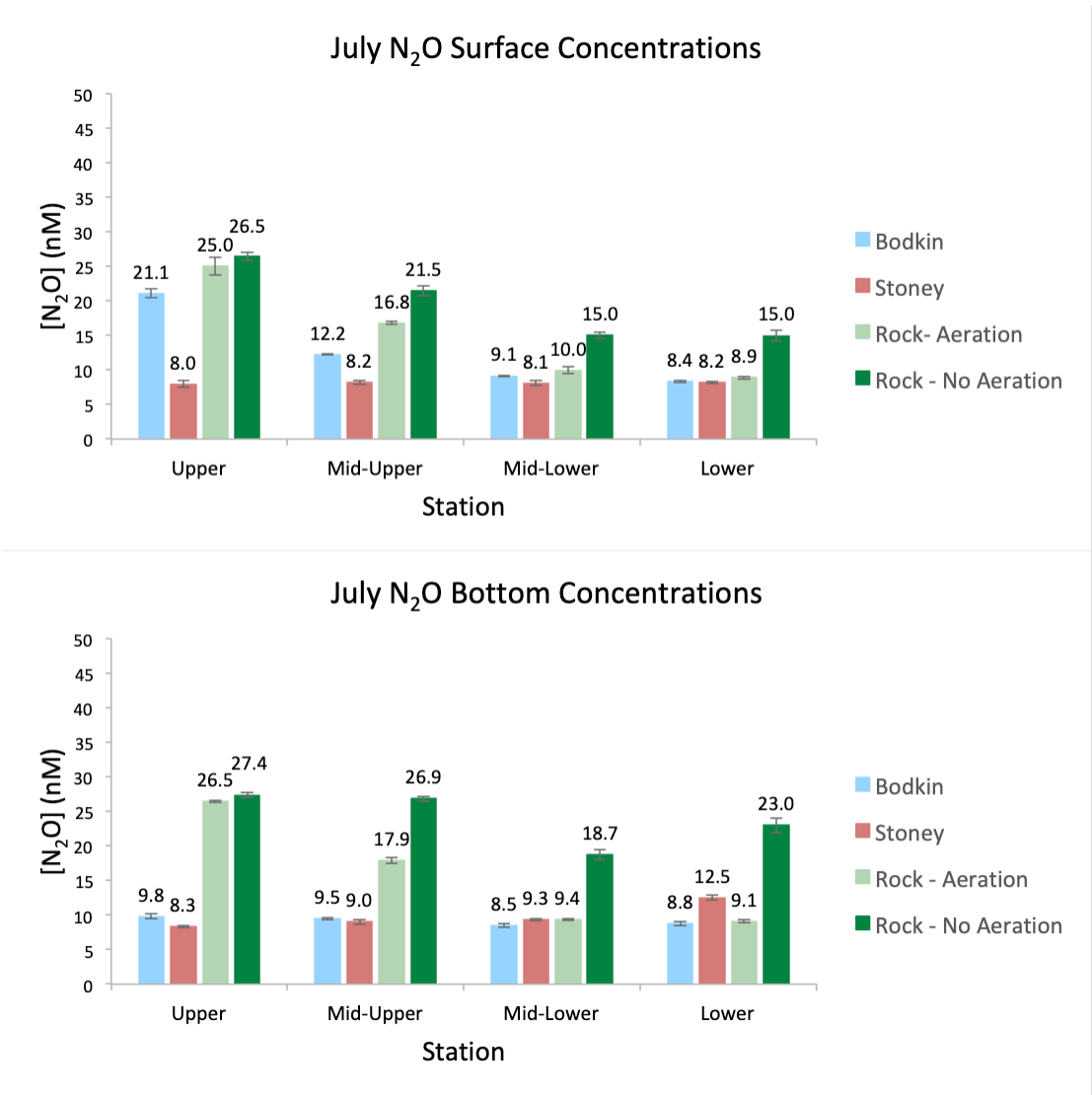

Figure 2.9 July surface and bottom water N_2O concentrations (nM) for Bodkin Creek, Stoney Creek, and Rock Creek. Peak N_2O concentrations are observed in Rock Creek bottom waters. All waters were above atmospheric N_2O equilibrium.

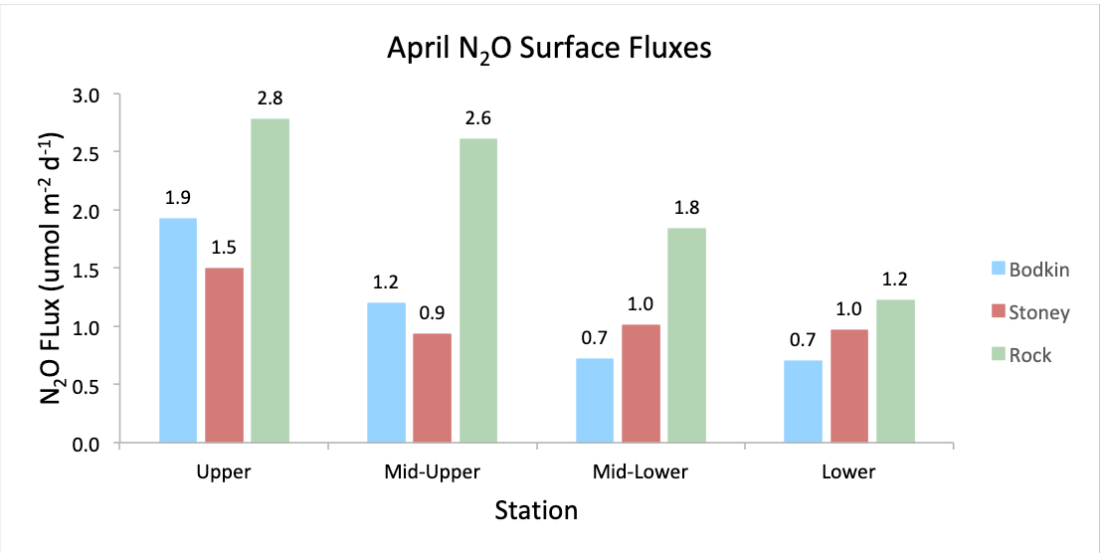

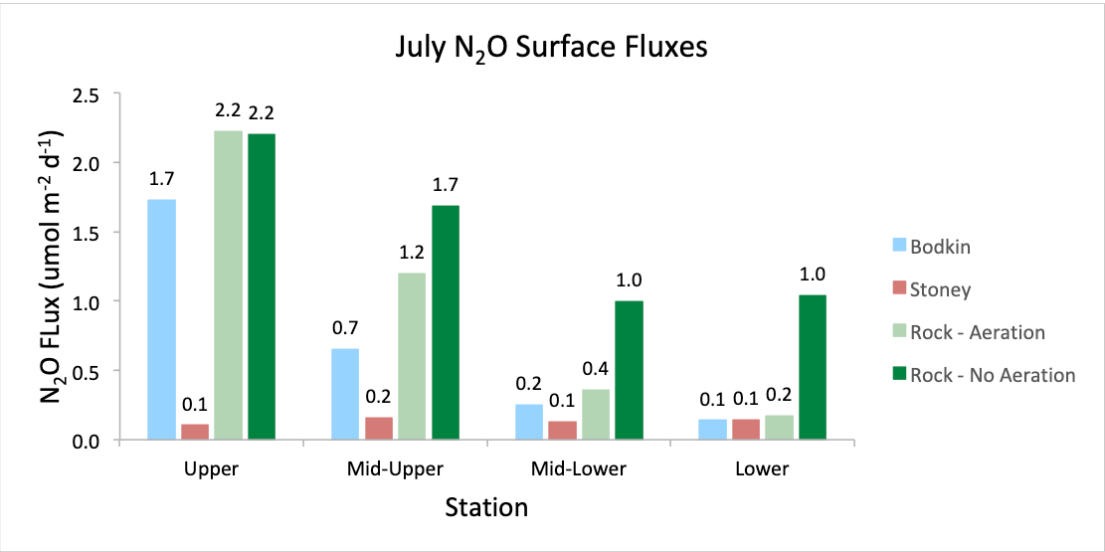

Figure 2.10 April and July surface N_2O fluxes (µmol m^{-2} d^{-1}) for Bodkin Creek, Stoney Creek, and Rock Creek. All creeks served as sources of N_2O to the atmosphere in April and July. Peak N_2O fluxes in April and July were measured in Rock Creek, consistent with elevated N_2O concentrations.

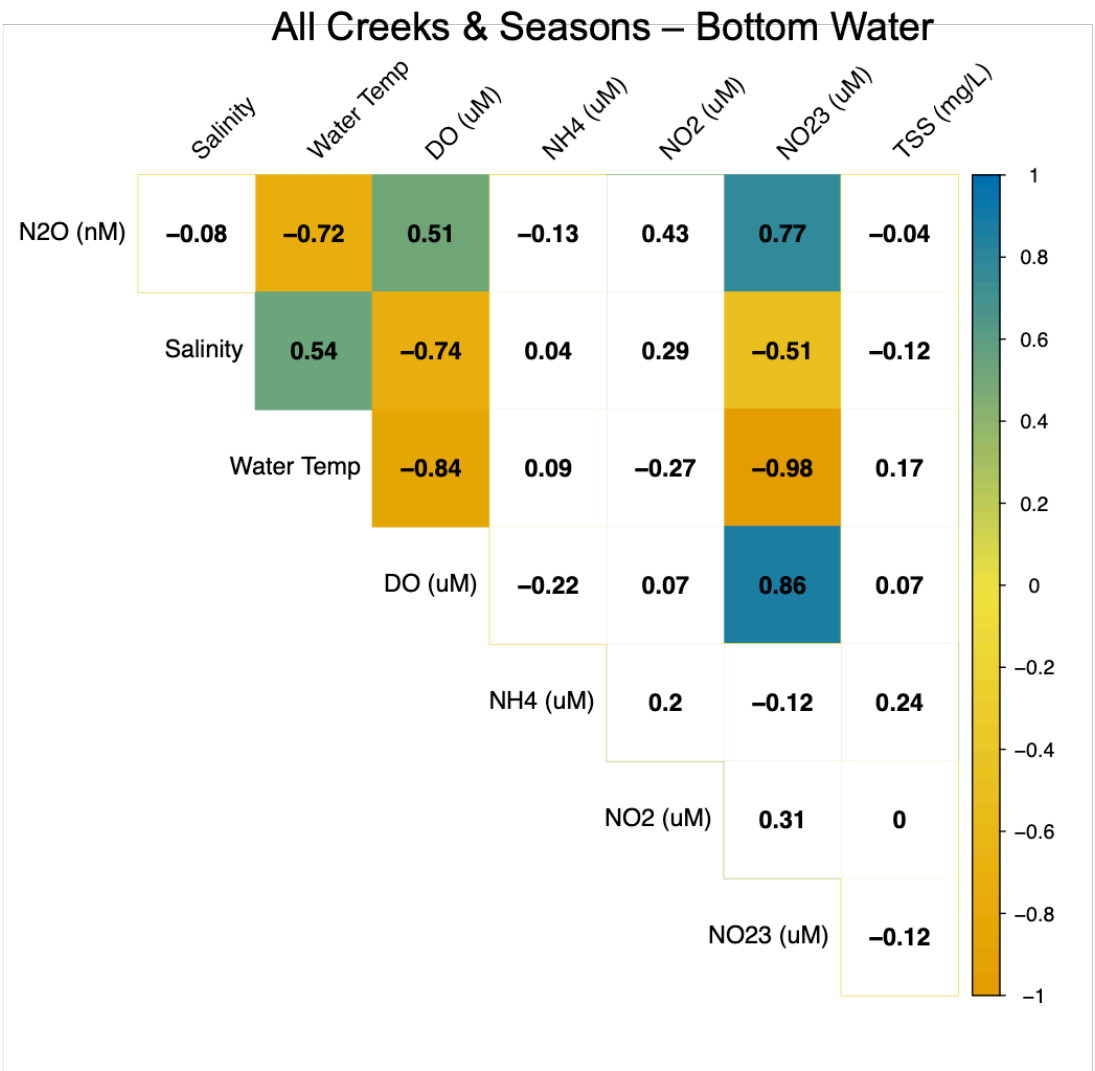

Figure 2.11 Correlation comparison for various water quality measurements. Data is aggregated for all creeks in April and July bottom waters. Highlighted cells represent significant correlations ($p<0.05$). Values within boxes represent correlation coefficients (Pearson method).

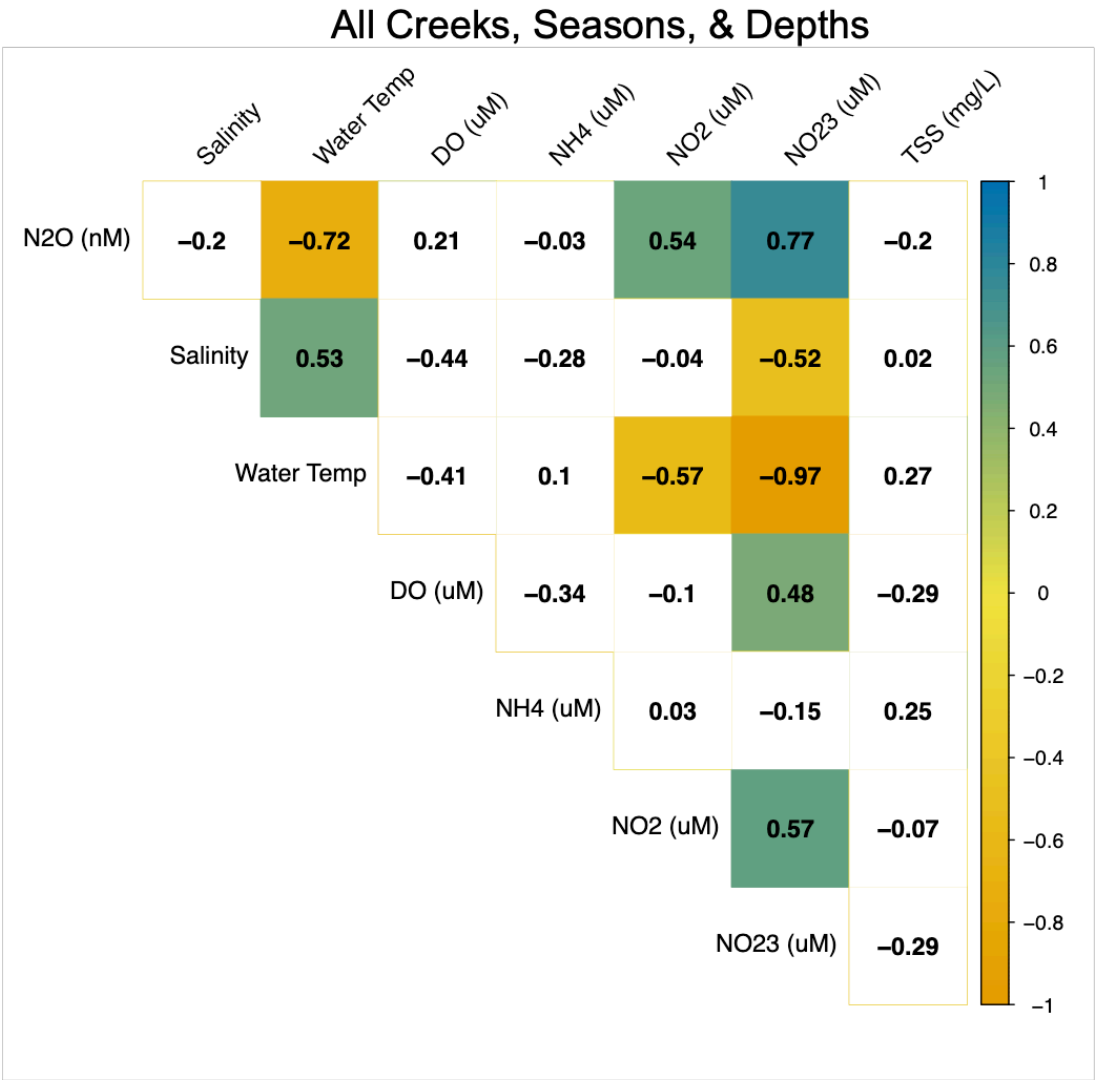

Figure 2.12 Correlation comparison for various water quality measurements. Data is aggregated for all creeks, seasons, and depths. Highlighted cells represent significant correlations ($p<0.05$). Values within boxes represent correlation coefficients (Pearson method).

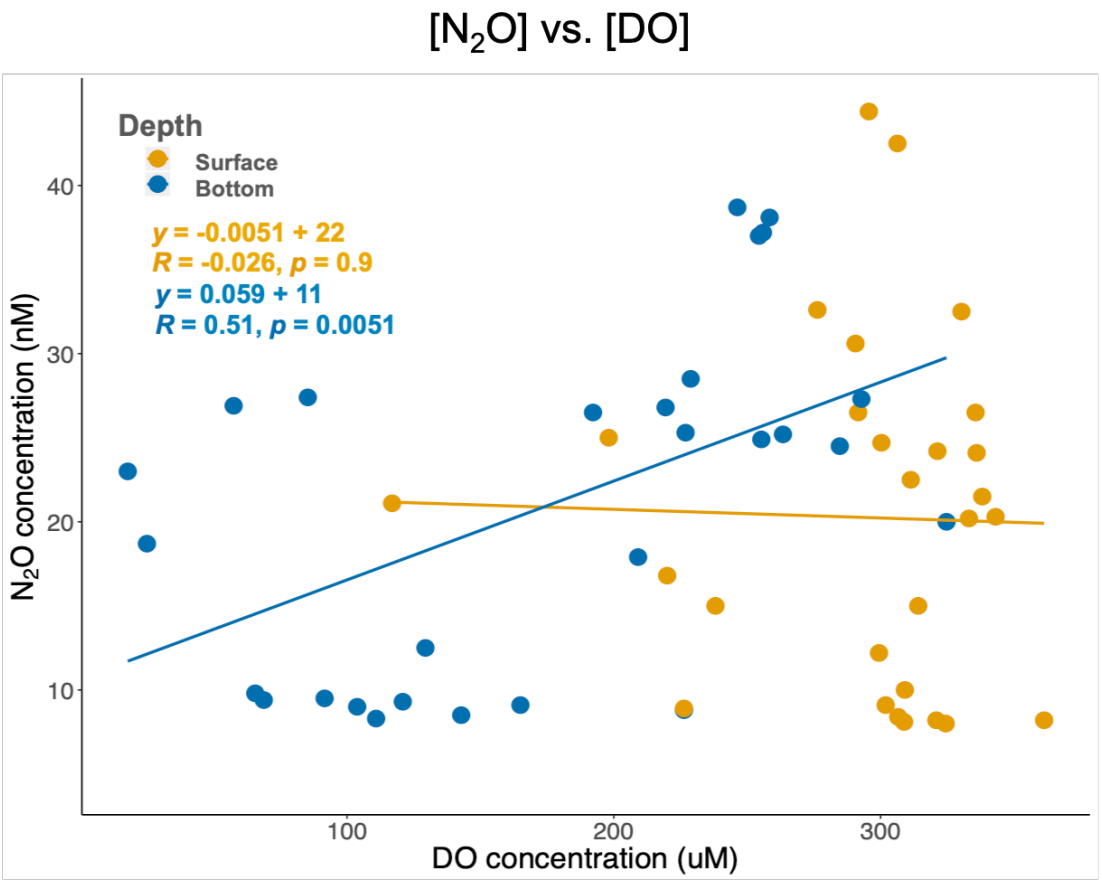

Figure 2.13 Relationship between N_2O concentration and DO concentration in surface and bottom waters in all creeks. Note significant correlation of N_2O and DO in bottom waters.

References

Andersen, T. K., Jensen, M. H., & Sørensen, J. (1984). Diurnal variation of nitrogen cycling in coastal, marine sediments. Marine Biology, 83(2), 171-176.

Armbruster, D. A., & Pry, T. (2008). Limit of blank, limit of detection and limit of quantitation. The clinical biochemist reviews, 29 (Suppl 1), S49.

Babbin, A. R., Bianchi, D., Jayakumar, A., & Ward, B. B. (2015). Rapid nitrous oxide cycling in the suboxic ocean. Science, 348(6239), 1127-1129.

Bange, H.W., S. Rapsomanikis, and M.O. Andreae. 1996. Nitrous oxide in coastal waters. Global Biogeochemical Cycles 10 (1): 197–207.

Bange, H. W., S. Rapsomanikis, S., and M.O. Andreae. 2001. Nitrous oxide cycling in the Arabian Sea, J. Geophys. Res.-Oceans 106: 1053– 1065.

Barnes, J., & Owens, N. J. P. (1999). Denitrification and nitrous oxide concentrations in the Humber estuary, UK, and adjacent coastal zones. Marine Pollution Bulletin, 37(3-7), 247-260.

Becker, K. H., Lörzer, J. C., Kurtenbach, R., Wiesen, P., Jensen, T. E., & Wallington, T. J. (1999). Nitrous oxide (N2O) emissions from vehicles. Environmental science & technology, 33(22), 4134-4139.

Berounsky, V. M., & Nixon, S. W. (1993). Rates of nitrification along an estuarine gradient in Narragansett Bay. Estuaries, 16(4), 718-730.

Billen, G. (1978). A budget of nitrogen recycling in North Sea sediments off the Belgian coast. Estuarine and Coastal Marine Science, 7(2), 127-146.

Blackburne, R., Yuan, Z., & Keller, J. (2008). Partial nitrification to nitrite using low dissolved oxygen concentration as the main selection factor. Biodegradation, 19(2), 303-312

Bonin, P., Tamburini, C., & Michotey, V. (2002). Determination of the bacterial processes which are sources of nitrous oxide production in marine samples. Water Research, 36(3), 722-732.

Bourbonnais, A., Letscher, R. T., Bange, H. W., Echevin, V., Larkum, J., Mohn, J., ... & Altabet, M. A. (2017). N_2O production and consumption from stable isotopic and concentration data in the Peruvian coastal upwelling system. Global Biogeochemical Cycles, 31(4), 678-698.

Boynton, W. R., Hagy, J. D., Cornwell, J. C., Kemp, W. M., Greene, S. M., Owens, M. S., ... & Larsen, R. K. (2008). Nutrient budgets and management actions in the Patuxent River estuary, Maryland. Estuaries and Coasts, 31(4), 623-651.

Boynton, W.R., and W.M. Kemp. 2008. Estuaries. In Nitrogen in the marine environment, ed. D.G. Capone, D.A. Bronk, M.R. Mulholland and E.J. Carpenter, 809-866. Amsterdam: Elsevier.

Brady, D. C., J.M. Testa, D.M. Di Toro, W.R. Boynton, and W.M. Kemp, 2013. Sediment flux modeling: Calibration and application for coastal systems. Estuarine, Coastal and Shelf Science.
117: 107-124.

Breitburg, D. L., Adamack, A., Rose, K. A., Kolesar, S. E., Decker, B., Purcell, J. E., ... & Cowan, J. H. (2003). The pattern and influence of low dissolved oxygen in the Patuxent River, a seasonally hypoxic estuary. Estuaries, 26(2), 280-297.

Brezonik, P. L., & Lee, G. F. (1966). Preservation of water samples for inorganic nitrogen analyses with mercuric chloride. Air and water pollution, 10(8), 549-553.

Buchwald, C., Santoro, A. E., McIlvin, M. R., & Casciotti, K. L. (2012). Oxygen isotopic composition of nitrate and nitrite produced by nitrifying cocultures and natural marine assemblages. Limnology and Oceanography, 57(5), 1361-1375.

Cai, W. J., & Sayles, F. L. (1996). Oxygen penetration depths and fluxes in marine sediments. Marine Chemistry, 52(2), 123-131

Capelle, D. W., Hawley, A. K., Hallam, S. J., & Tortell, P. D. (2018). A multi‐year time‐series of N2O dynamics in a seasonally anoxic fjord: Saanich Inlet, British Columbia. Limnology and Oceanography, 63(2), 524-539.

Cole, Jonathan J., and Nina F. Caraco. "Emissions of nitrous oxide (N2O) from a tidal, freshwater river, the Hudson River, New York." Environmental science & technology 35.6 (2001): 991-996.

Cooper, L. H. N. (1933). Chemical Constituents of Biological Importance in the English Channel, November, 1930, to January, 1932. Part I. Phosphate, silicate, nitrate, nitrite, ammonia. Journal of the Marine Biological Association of the United Kingdom, 18(2), 677-728.

Cornwell, J. C., Owens, M. S., Boynton, W. R., & Harris, L. A. (2015). Sediment-water nitrogen exchange along the Potomac River estuarine salinity gradient. Journal of Coastal Research, 32(4), 776-787.

Cronin, W. B. (1971). Volumetric, areal, and tidal statistics of the Chesapeake Bay Estuary and its tributaries. Special Report 20. Chesapeake Bay Institute, The Johns Hopkins University. Reference 71-2. Baltimore, Maryland.

Cronin, W. B., & Pritchard, D. W. (1975). Additional statistics on the dimensions of the Chesapeake Bay and its tributaries: Cross-section widths and segment volumes per meter depth. Special Report 42. Chesapeake Bay Institute, The Johns Hopkins University. Reference 75-3. Baltimore, Maryland.

Crutzen, P. J. (1970). The influence of nitrogen oxides on the atmospheric ozone content.Quarterly Journal of the Royal MeteorologicalSociety,96(408), 320–325. https://doi.org/10.1002/qj.49709640815

Davidson, E. A. (2009). The contribution of manure and fertilizer nitrogen to atmospheric nitrous oxide since 1860. Nature Geoscience, 2(9), 659.

de Wilde, H.P.J, and MJ.M de Bie. 2000. Nitrous oxide in the Schelde estuary: production by nitrification and emission to the atmosphere. Marine Chemistry 69: 203–216.

Deck, B.L., 1981. Nutrient element distribution in the Hudson estuary, PhD Dissertation, Columbia University, New York, 396 pp.

Di Toro, D. M. 2001. Sediment flux modeling (Vol. 116). New York: Wiley-Interscience.

Dones, R., Heck, T., & Hirschberg, S. (2004). Greenhouse gas emissions from energy systems: comparison and overview (No. CH--0401).

Dong, L. F., Nedwell, D. B., Colbeck, I., & Finch, J. (2005). Nitrous oxide emission from some English and Welsh rivers and estuaries. Water, Air, & Soil Pollution: Focus, 4(6), 127-134.

Elkins, J.W., S.C. Wofsy, M.B. McElroy, C.E. Kolb, and W.A. Kaplan. 1978. Aquatic sources and sinks for nitrous oxide. Nature 275 (5681): 602–606.

Elkins, J.W. 1980. Determination of dissolved nitrous oxide in aquatic systems by gas chromatography using electron-capture detection and multiple phase equilibration. Analytical Chemistry 52 (2): 263–267.

Farías, L., & Cornejo, M. (2007). Effect of seasonal changes in bottom water oxygenation on sediment N oxides and N2O cycling in the coastal upwelling regime off central Chile (36.5 S). Progress in Oceanography, 75(3), 561-575.

Farías, L., Castro-González, M., Cornejo, M., Charpentier, J., Faúndez, J., Boontanon, N., & Yoshida, N. (2009). Denitrification and nitrous oxide cycling

within the upper oxycline of the eastern tropical South Pacific oxygen minimum zone. Limnology and Oceanography, 54(1), 132-144.

Fisher, T. R., Hagy, J. I. D., Boynton, W. R., & Williams, M. R. (2006). Cultural eutrophication in the Choptank and Patuxent estuaries of Chesapeake Bay. Limnology and Oceanography, 51(1part2), 435-447.

Frame, C. H., & Casciotti, K. L. (2010). Biogeochemical controls and isotopic signatures of nitrous oxide production by a marine ammonia-oxidizing bacterium.

Galloway, J. N., Schlesinger, W. H., Levy, H., Michaels, A., & Schnoor, J. L. (1995). Nitrogen fixation: Anthropogenic enhancement‐environmental response. Global biogeochemical cycles, 9(2), 235-252

Garnier, J., Cébron, A., Tallec, G., Billen, G., Sebilo, M., & Martinez, A. (2006). Nitrogen behaviour and nitrous oxide emission in the tidal Seine River estuary (France) as influenced by human activities in the upstream watershed. Biogeochemistry, 77(3), 305-326.

Gloël, J., Robinson, C., Tilstone, G. H., Tarran, G., & Kaiser, J. (2015). Could benzalkonium chloride be a suitable alternative to mercuric chloride for preservation of seawater samples?. Ocean Science Discussions, 12(4), 1953-1969.

Goreau, T.J., Kaplan, W.A., Wofsy, S.C., McElroy, M.B., Valois, F.W., Watson, S.W., 1980. Production of NO2- and N2O by nitrifying bacteria at reduced concentrations of oxygen. Appl. Environ. Microbiol. 40, 526–532.

Greene, S.E., 2005, Tidal fresh and oligohaline marshes as nutrient sinks in the upper Patuxent River estuary. MS thesis, University of MD.

Hanaki, K., Hong, Z., & Matsuo, T. (1992). Production of nitrous oxide gas during denitrification of wastewater. Water Science and Technology, 26(5-6), 1027-1036.

Hansen, J. I., Henriksen, K., & Blackburn, T. H. (1981). Seasonal distribution of nitrifying bacteria and rates of nitrification in coastal marine sediments. Microbial Ecology, 7(4), 297-304.

Harris, L.A., Hodgkins, C. L. S., Day, M. C., Austin, D., Testa, J. M., Boynton, W., ... & Chen, N. W. (2015). Optimizing recovery of eutrophic estuaries: impact of destratification and re-aeration on nutrient and dissolved oxygen dynamics. Ecological Engineering, 75, 470-483.

Harris, L.A., Testa, J.M. (2019). Quantifying changes to nutrient cycling and nitrogen removal in an estuary as a consequence of aeration. (Report No. TS-742-19). Solomons, MD: University of Maryland Center for Environmental Science Chesapeake Biological Laboratory.

Henriksen, K. (1980). Measurement of in situ rates of nitrification in sediment. Microbial Ecology, 6(4), 329-337.

Henriksen, K., Hansen, J. I., & Blackburn, T. H. (1981). Rates of nitrification, distribution of nitrifying bacteria, and nitrate fluxes in different types of sediment from Danish waters. Marine Biology, 61(4), 299-304.

Homer, C., Dewitz, J., Fry, J., Coan, M., Hossain, N., Larson, C., ... & Wickham, J. (2007). Completion of the 2001 national land cover database for the counterminous United States. Photogrammetric engineering and remote sensing, 73(4), 337.

Hu, H. W., Chen, D., & He, J. Z. (2015). Microbial regulation of terrestrial nitrous oxide formation: understanding the biological pathways for prediction of emission rates. FEMS microbiology reviews, 39(5), 729-749.

IPCC, 2007: Climate Change 2007: Synthesis Report. Contribution of Working Groups I, II and III to the Fourth Assessment Report of the Intergovernmental Panel on Climate Change [Core Writing Team, Pachauri, R.K and Resinger, A. (eds.)]. IPCC, Geneva, Switzerland, 104 pp.

IPCC, 2013: Climate Change 2013: The Physical Science Basis. Contribution of Working Group I to the Fifth Assessment Report of the Intergovernmental Panel on Climate Change [Stocker, T.F., D. Qin, G.-K. Plattner, M. Tignor, S.K. Allen, J. Boschung, A. Nauels, Y. Xia, V. Bex and P.M. Midgley (eds.)]. Cambridge University Press, Cambridge, United Kingdom and New York, NY, USA, 1535 pp, doi:10.1017/CBO9781107415324.

Jenkins, M. C., & Kemp, W. M. (1984). The coupling of nitrification and denitrification in two estuarine sediments 1, 2. Limnology and Oceanography, 29(3), 609-619.

Jensen, H. B., Jørgensen, K. S., & Sørensen, J. (1984). Diurnal variation of nitrogen cycling in coastal, marine sediments. Marine Biology, 83(2), 177-183.

Ji, Qixing, A.R. Babbin, A. Jayakumar, S. Oleynik, and B.B. Ward. 2015. Nitrous oxide production by nitrification and denitrification in the eastern tropical South Pacific oxygen minimum zone. Geophysical Research Letters 42 (24): 10,755–10,764.

Ji, Qixing., C. Frey, X. Sun, M. Jackson, Y.S. Lee, A. Jayakumar, J.C. Cornwell, B.B. Ward. 2018. Nitrogen and oxygen availabilities control water column nitrous oxide production during seasonal anoxia in the Chesapeake Bay. Biogeosciences 15: 6127-6138.

Jianlong, W., & Ning, Y. (2004). Partial nitrification under limited dissolved oxygen conditions. Process Biochemistry, 39(10), 1223-1229.

Kana, T. M., Darkangelo, C., Hunt, M. D., Oldham, J. B., Bennett, G. E., & Cornwell, J. C. (1994). Membrane inlet mass spectrometer for rapid high-precision determination of N2, O2, and Ar in environmental water samples. Analytical Chemistry, 66(23), 4166-4170.

Kemp, W. M., Sampou, P., Caffrey, J., Mayer, M., Henriksen, K., & Boynton, W. R. (1990). Ammonium recycling versus denitrification in Chesapeake Bay sediments. Limnology and Oceanography, 35(7), 1545-1563.

Kemp, W.M., J.M. Testa,, D.J. Conley, D. Gilbert, H.D. and Hagy. 2009. Temporal responses of coastal hypoxia to nutrient loading and physical controls. Biogeosciences 6: 2985-3008.

Knowles, R. (1982). Denitrification. Microbiological reviews, 46(1), 43.

LaMontagne, M. G., Duran, R., & Valiela, I. (2003). Nitrous oxide sources and sinks in coastal aquifers and coupled estuarine receiving waters. Science of the Total Environment, 309(1-3), 139-149.

Lansdown, K., Trimmer, M., Heppell, C. M., Sgouridis, F., Ullah, S., Heathwaite, A. L., ... & Zhang, H. (2012). Characterization of the key pathways of dissimilatory nitrate reduction and their response to complex organic substrates in hyporheic sediments. Limnology and Oceanography, 57(2), 387-400.

Laperriere, S. M., Nidzieko, N. J., Fox, R. J., Fisher, A. W., & Santoro, A. E. (2019). Observations of Variable Ammonia Oxidation and Nitrous Oxide Flux in a Eutrophic Estuary. Estuaries and coasts, 42(1), 33-44.

Ligi, T., Truu, M., Truu, J., Nõlvak, H., Kaasik, A., Mitsch, W. J., & Mander, Ü. (2014). Effects of soil chemical characteristics and water regime on denitrification genes (nirS, nirK, and nosZ) abundances in a created riverine wetland complex. Ecological Engineering, 72, 47-55

Liu, X. L., Bai, L., Wang, Z. L., Li, J., Yue, F. J., & Li, S. L. (2015). Nitrous oxide emissions from river network with variable nitrogen loading in Tianjin, China. Journal of Geochemical Exploration, 157, 153-161.

Magalhães, C. M., Joye, S. B., Moreira, R. M., Wiebe, W. J., & Bordalo, A. A. (2005). Effect of salinity and inorganic nitrogen concentrations on nitrification and denitrification rates in intertidal sediments and rocky biofilms of the Douro River estuary, Portugal. Water Research, 39(9), 1783-1794.

McElroy, M. B., Elkins, J. W., Wofsy, S. C., Kolb, C. E., Duran, A. P., & Kaplan, W. A. (1978). Production and release of N2O from the Potomac Estuary 1. Limnology and Oceanography, 23(6), 1168-1182.

Merrill, J. Z., & Cornwell, J. C. (2002). The role of oligohaline marshes in estuarine nutrient cycling. In Concepts and controversies in tidal marsh ecology (pp. 425-441). Springer, Dordrecht.

Middelburg, J. J., Klaver, G., Nieuwenhuize, J., Markusse, R. M., Vlug, T., & van der Nat, F. J. W. (1995). Nitrous oxide emissions from estuarine intertidal sediments. Hydrobiologia, 311(1-3), 43-55.

Moore, W. S. (1999). The subterranean estuary: a reaction zone of ground water and sea water. Marine Chemistry, 65(1-2), 111-125.

Mosier, A. R., Duxbury, J. M., Freney, J. R., Heinemeyer, O., & Minami, K. (1998). Assessing and mitigating N2O emissions from agricultural soils. Climatic change, 40(1), 7-38.

Murray, R. H., Erler, D. V., & Eyre, B. D. (2015). Nitrous oxide fluxes in estuarine environments: response to global change. Global change biology, 21(9), 3219-3245.

Naqvi, S. W. A., Bange, H. W., Farías, L., Monteiro, P. M. S., Scranton, M. I., & Zhang, J. (2010). Marine hypoxia/anoxia as a source of CH4 and N2O. Biogeosciences, 7(7), 2159-2190.

Nielsen, T. H., Nielsen, L. P., & Revsbech, N. P. (1996). Nitrification and coupled nitrification-denitrification associated with a soil-manure interface. Soil Science Society of America Journal, 60(6), 1829-1840.

Nishio, T., Koike, I., & Hattori, A. (1982). Denitrification, nitrate reduction, and oxygen consumption in coastal and estuarine sediments. Appl. Environ. Microbiol., 43(3), 648-653.

Nevison, C., Butler, J. H., & Elkins, J. W. (2003). Global distribution of N2O and the ΔN2O–AOU yield in the subsurface ocean. Global Biogeochemical Cycles, 17(4).

Oh, J., & Silverstein, J. (1999). Oxygen inhibition of activated sludge denitrification. Water Research, 33(8), 1925-1937.

Otte, S., Grobben, N. G., Robertson, L. A., Jetten, M. S., & Kuenen, J. G. (1996). Nitrous oxide production by Alcaligenes faecalis under transient and dynamic aerobic and anaerobic conditions. Appl. Environ. Microbiol., 62(7), 2421-2426.

Palta, M. M., Ehrenfeld, J. G., & Groffman, P. M. (2013). Denitrification and potential nitrous oxide and carbon dioxide production in brownfield wetland soils. Journal of environmental quality, 42(5), 1507-1517.

Parravicini, V., Svardal, K., & Krampe, J. (2016). Greenhouse gas emissions from wastewater treatment plants. Energy Procedia, 97, 246-253.

Pérez-Villalona, H., Cornwell, J. C., Ortiz-Zayas, J. R., & Cuevas, E. (2015). Sediment denitrification and nutrient fluxes in the San José Lagoon, a tropical lagoon in the highly urbanized San Juan Bay Estuary, Puerto Rico. Estuaries and coasts, 38(6), 2259-2278.

Punshon, S., & Moore, R. M. (2004). Nitrous oxide production and consumption in a eutrophic coastal embayment. Marine chemistry, 91(1-4), 37-51.

Quick, A. M., W. J. Reeder, T. B. Farrell, D. Tonina, K. P. Feris, and S. G. Benner. 2019. Nitrous oxide from streams and rivers: A review of primary biogeochemical pathways and environmental variables. Earth-Science Reviews 191: 224-262.

Rajkumar, A. N., Barnes, J., Ramesh, R., Purvaja, R., & Upstill-Goddard, R. C. (2008). Methane and nitrous oxide fluxes in the polluted Adyar River and estuary, SE India. Marine Pollution Bulletin, 56(12), 2043-2051.

Santoro, A. E., Casciotti, K. L., & Francis, C. A. (2010). Activity, abundance and diversity of nitrifying archaea and bacteria in the central California Current. Environmental Microbiology, 12(7), 1989-2006.

Santoro, Alyson E., Carolyn Buchwald, Matthew R. McIlvin, and Karen L. Casciotti. 2011. Isotopic signature of N2O produced by marine ammonia-oxidizing archaea. Science 333 (6047): 1282–1285. https://doi.org/10.1126/science.1208239.

Schipper, L. A., Barkle, G. F., & Vojvodic-Vukovic, M. (2005). Maximum rates of nitrate removal in a denitrification wall. Journal of environmental quality, 34(4), 1270-1276.

Sebilo, M., Billen, G., Mayer, B., Billiou, D., Grably, M., Garnier, J., & Mariotti, A. (2006). Assessing nitrification and denitrification in the Seine River and estuary using chemical and isotopic techniques. Ecosystems, 9(4), 564-577.

Seitzinger, S. P. (1988). Denitrification in freshwater and coastal marine ecosystems: ecological and geochemical significance. Limnology and Oceanography, 33(4part2), 702-724.

Seitzinger, S., S. Nixon, M. E. Q. Pilson, and S. Burke. 1980. Denitrification and N_2O production in near-shore marine-sediments. Geochimica Et Cosmochimica Acta 44: 1853-1860.

Seitzinger, Sybil P., and Carolien Kroeze. 1998. Global distribution of nitrous oxide production and N inputs in freshwater and coastal marine ecosystems. Global Biogeochemical Cycles 12 (1): 93–113. https://doi.org/10.1029/97GB03657.

Sellner, K. G., Sellner, S. G., Lacouture, R. V., & Magnien, R. E. (2001). Excessive nutrients select for dinoflagellates in the stratified Patapsco River estuary: Margalef reigns. Marine Ecology Progress Series, 220, 93-102.

Smith, M. S. (1982). Dissimilatory Reduction of NO2− to NH4+ and N2O by a Soil Citrobacter sp. Appl. Environ. Microbiol., 43(4), 854-860.

Stein, L. Y., & Yung, Y. L. (2003). Production, isotopic composition, and atmospheric fate of biologically produced nitrous oxide. Annual Review of Earth and Planetary Sciences, 31(1), 329-356.

Strauss, E. A., Richardson, W. B., Bartsch, L. A., Cavanaugh, J. C., Bruesewitz, D. A., Imker, H., ... & Soballe, D. M. (2004). Nitrification in the Upper Mississippi River: patterns, controls, and contribution to the NO3− budget. Journal of the North American Benthological Society, 23(1), 1-14.

Sweeney, C., Gloor, E., Jacobson, A. R., Key, R. M., McKinley, G., Sarmiento, J. L., & Wanninkhof, R. (2007). Constraining global air‐sea gas exchange for CO2 with recent bomb 14C measurements. Global Biogeochemical Cycles, 21(2).

Sun, Y., De Vos, P., & Willems, A. (2018). Influence of nitrate and nitrite concentration on N2O production via dissimilatory nitrate/nitrite reduction to ammonium in Bacillus paralicheniformis LMG 6934. MicrobiologyOpen, 7(4), e00592.

Suntharalingam, P., Buitenhuis, E., Le Quéré, C., Dentener, F., Nevison, C., Butler, J. H., ... & Forster, G. (2012). Quantifying the impact of anthropogenic nitrogen deposition on oceanic nitrous oxide. Geophysical Research Letters, 39(7).

Syakila, A., & Kroeze, C. (2011). The global nitrous oxide budget revisited. Greenhouse Gas Measurement and Management, 1(1), 17-26.

Takahashi, T., Broecker, W. S., & Langer, S. (1985). Redfield ratio based on chemical data from isopycnal surfaces. Journal of Geophysical Research: Oceans, 90(C4), 6907-6924.

Testa, J.M., D.C. Brady, D.M. Di Toro, W.R. Boynton, W.M. Boynton. 2013. Sediment flux modeling: simulating nitrogen, phosphorus and silica cycles. Estuarine, Coastal and Shelf Science 131: 245-263.

Testa, J.M. and W.M. Kemp. 2012. Hypoxia-induced shifts in nitrogen and phosphorus cycling in Chesapeake Bay. Limnology and Oceanography. 57: 835–850.

Testa, J. M., Kemp, W. M., Boynton, W. R., & Hagy, J. D. (2008). Long-term changes in water quality and productivity in the Patuxent River estuary: 1985 to 2003. Estuaries and Coasts, 31(6), 1021-1037.

Testa, J.M., R.R. Murphy, D.C. Brady, and W.M. Kemp. 2018. Nutrient-and climate-induced shifts in the phenology of linked biogeochemical cycles in a temperate

estuary. Frontiers in Marine Science 5: 1–15.

Thompson, R. L., Lassaletta, L., Patra, P. K., Wilson, C., Wells, K. C., Gressent, A., ... & Tian, H. (2019). Acceleration of global N 2 O emissions seen from two decades of atmospheric inversion. Nature Climate Change, 1-6.

Tiedje, J. M. (1988). Ecology of denitrification and dissimilatory nitrate reduction to ammonium. Biology of anaerobic microorganisms, 717, 179-244.

USEPA (United States Environmental Protection Agency). (2010). Chesapeake Bay Total Maximum Daily Load for Nitrogen, Phosphorus and Sediment.

Upstill-Goddard, R. C., A.P. Rees, and N.J.P. Owens. 1996. Simultaneous high-precision measurements of methane and nitrous oxide in water and seawater by single phase equilibration gas chromatography, Deep-Sea Res. 43: 1669–1682.

Von Schulthess, R., Wild, D., & Gujer, W. (1994). Nitric and nitrous oxides from denitrifying activated sludge at low oxygen concentration. Water Science and Technology, 30(6), 123.

Walter, S., Bange, H. W., Breitenbach, U., and Wallace, D. W. R.: Nitrous oxide in the North Atlantic Ocean, Biogeosciences, 3, 607–619, https://doi.org/10.5194/bg-3-607-2006, 2006

Wanninkhof, R. (2014). Relationship between wind speed and gas exchange over the ocean revisited. Limnology and Oceanography: Methods, 12(6), 351-362.

Weiss, R. F., F.A. Van Woy, and P.K. Salameh. 1992. Surface water and atmospheric carbon dioxide and nitrous oxide observation by shipboard automated gas chromatography: Results from expeditions between 1977 and 1990, Scripps Institution of oceanography Reference 92-11, ORNL/CDIAC-59, NDP-044, Carbon Dioxide Information Analysis Center, Oak Ridge National Laboratory, Tennessee.

Williams, M. R., Fisher, T. R., Boynton, W. R., Cerco, C. F., Kemp, M. W., Eshleman, K. N., ... & Radcliffe, G. R. (2006). An integrated modelling system for management of the Patuxent River estuary and basin, Maryland, USA. International Journal of Remote Sensing, 27(17), 3705-3726.

Wilson, S.T., and others. 2018. An intercomparison of oceanic methane and nitrous oxide measurements. Biogeosciences. 15: 5891-5907. doi:https://doi.org/10.5194/bg-15-5891-2018.

Wuebbles, D. J. (2009). Nitrous oxide: no laughing matter. Science, 326(5949), 56-57.

Yoshinari, T. (1976). Nitrous oxide in the sea. Marine Chemistry, 4(2), 189-202.

Yoshinari, T., Altabet, M. A., Naqvi, S. W. A., Codispoti, L., Jayakumar, A., Kuhland, M., & Devol, A. (1997). Nitrogen and oxygen isotopic composition of N2O from suboxic waters of the eastern tropical North Pacific and the Arabian Sea—Measurement by continuous-flow isotope-ratio monitoring. Marine Chemistry, 56(3-4), 253-264.

Yu, T., & Zhuang, Q. (2019). Quantifying global N 2 O emissions from natural ecosystem soils using trait-based biogeochemistry models. Biogeosciences, 16(2), 207-222.

Zhang, G., Zhang, J., Ren, J., Li, J., & Liu, S. (2008). Distributions and sea-to-air fluxes of methane and nitrous oxide in the North East China Sea in summer. Marine Chemistry, 110(1-2), 42-55.